Science of Remote Sensing 4 (2021) 100025

Contents lists available at ScienceDirect

Science of Remote Sensing

journal homepage: www.sciencedirect.com/journal/science-of-remote-sensing

Revisiting the use of red and near-infrared reflectances in vegetation studies and numerical climate models

Garik Gutman [a,*], Sergii Skakun [b], Anatoly Gitelson [c,d]

[a] NASA Headquarters (HQ), Washington, DC, 20546, USA
[b] Department of Geographical Sciences, University of Maryland, College Park, MD, 20742, USA
[c] School of Natural Resources, University of Nebraska-Lincoln, Lincoln, NE, 68583, USA
[d] Israel Institute of Technology (Technion), Haifa, 3200003, Israel

ARTICLE INFO

Keywords:
Optical remote sensing form satellites
Surface reflectances
Vegetation monitoring
Chlorophyll
Leaf area index
FPAR
Climate models
Parameterization
Crop types

ABSTRACT

Surface reflectance data acquired in red and near-infrared spectra by remote sensing sensors are traditionally applied to construct various vegetation indices (VIs), which are related to vegetation biophysical parameters. Most VIs use pre-defined weights (usually equal to 1) for the red and NIR reflectance values, therefore constraining particular weights for red and NIR during the VI design phase, and potentially limiting capabilities of the VI to explain an independent variable. In this paper, we propose an approach to estimate biophysical variables, such as Leaf Area Index (LAI), Canopy Chlorophyll Content (CCC) and Fraction of Photosynthetically Active Radiation (FPAR) absorbed by green vegetation, represented as linear combinations of the red and NIR reflectances with weights determined empirically from observations and radiative transfer model (PROSAIL) simulations. The proof of concept is first tested on available close-range observations over maize and soybean crops in Nebraska, USA. The empirical results compare well with those from PROSAIL model simulations. The proposed LAI model is then used with data from Landsat 8, Sentinel-2 and Planet/Dove, and the results are validated with in situ LAI measurements in Ukraine. We show that the weights on red and NIR reflectances are vegetation-specific and stable in time. The approach is further tested on crops and forests in the conterminous USA and on a global scale using MODIS LAI and FPAR products as proxies for "ground observations". These LAI and FPAR, however, are not independently measured but derived from the corresponding remotely sensed reflectances, which precludes recommending a final set of the weights/coefficients for the users, and, thus, should be considered mostly for demonstrating the concept. The results for crop types, other than maize and soybean, and for all forests are conceptual and need to be tested with real ground data. It was, however, encouraging to see that the derived maps of coefficients/weights exhibit regular patterns over the globe compatible with those of vegetation classes and crop types. Tedious and thorough work on compiling available in situ measurements on various crops and forests needs to be accomplished prior to large-scale applications, and the method needs to be further tested and proven that it works at a large scale.

The proposed parameterization may be attractive for global studies of various sub-classes of vegetation, once the parameter coefficients are established, validated, tabulated and their stability verified. Ultimately, this approach may provide quantification of vegetation traits for the past decades and be a useful asset for climate models that include satellite-derived land cover classifications and vegetation variables for simulating surface fluxes.

This is a conceptual paper, with a proof-of-concept supported by observations over two crops, for which we had close-range observations. It is not a technical note, which would provide users with a recommended set of coefficients for global applications. Our intent was to develop a paradigm, which could ultimately be useful in global models.

* Corresponding author. NASA Headquarters, Mail Suite 3V73 Room 3Y77, 300 E Street, SW, Washington, DC, 20546, USA.
E-mail addresses: garik.gutman@nasa.gov, ggutman@nasa.gov (G. Gutman).

https://doi.org/10.1016/j.srs.2021.100025
Received 10 March 2021; Received in revised form 18 June 2021; Accepted 22 June 2021
Available online 26 June 2021

1. Introduction

Methods for studying, modelling and monitoring vegetation range from using simple indices during the last several decades to a more recent intensified use of machine learning methods, such as neural networks and Gaussian processes (e.g., Reichstein et al., 2019). The use of vegetation indices, such as the Normalized Difference Vegetation Index (NDVI), can be explained by their simplicity and the level of methodologies and technologies at the time they were introduced. Before its use with satellite data, NDVI was developed for studying vegetation traits at close range using hand-held radiometers (Kriegler et al., 1969; Rouse et al., 1974). The reasoning and advantage of using the simple ratio vegetation index $RVI = \frac{\rho_2}{\rho_1}$, where ρ_2 and ρ_1 are reflectance values in near-infrared (NIR, ~0.8 μm) and red (~0.67 μm) spectra, or its function, NDVI, over the use of reflectances without combining them has been the fact that sun-target-sensor geometry and atmospheric effects are partially compensated in the ratio-based indices. This compensation made NDVI and RVI more attractive for use in vegetation studies and model parameterizations since 1980's following the seminal study by Sellers (1985). Also, the contrast between the green vegetation and the background (soil, dead vegetation) is emphasized when a combination of the observations in NIR and red bands is analyzed (e.g., Baret and Guyot, 1991). The use of NDVI derived from space observations, pioneered by Tucker (1979), has been justified for observations from the Advanced Very High Resolution Radiometer (AVHRR) because the methods for bi-directional and atmospheric corrections were not well developed at the early stages of AVHRR applications. However, during the past couple of decades, corrections have been applied to the next generation coarse-resolution scanning sensors after AVHRR, namely the Moderate Resolution Imaging Spectroradiometer (MODIS) and Visible Infrared Imaging Radiometer Suite (VIIRS) (Schaaf et al., 2002; Vermote and Kotchenova, 2008). Landsat, on the other hand, is a sensor with a close-to-nadir viewing geometry, hence vegetation studies with Landsat data have used linear combinations of reflectances in the so-called Tasseled-Cap Transformation (Kauth, 1976; Crist, 1985), but many researchers still calculate vegetation ratio indices from Landsat data, even though the atmospherically corrected surface reflectances are available as standard Landsat product (Vermote et al., 2016).

Most important vegetation traits, affecting water, energy and carbon fluxes at the surface-atmosphere interface, that can be derived from remote sensing observations are Leaf Area Index (LAI) and Fraction of Photosynthetically Active Radiation (FPAR) absorbed by green vegetation. Many studies in late '80s - early '90s stressed the necessity for including vegetation parameterizations within numerical weather prediction and climate models (e.g., Pielke et al., 1991). Since the seminal work by Deardorff (1978), land surface parameterizations commonly have included the effect of vegetation density (through LAI) and coverage through "vegetation green fraction" (Gutman and Ignatov, 1998) that provide critical information on the partitioning of the latent heat flux between unvegetated soil and canopy evapotranspiration and the Bowen ratio (Avissar, 1995).

The above biophysical variables are included in land surface parameterizations and radiative transfer schemes (e.g., Sellers et al., 1996; Carrer et al., 2013). Vegetation indices have been used extensively as their proxies in weather and climate prediction models since 1990's (Gutman 1990). An alternative approach could be a direct use of observed reflectances as input to a land surface parameterization if vegetation variables were parameterized by a simple model with prescribed coefficients (Avissar, 1995, personal communications). The current paper shows that a simple two-parametric model can provide a reasonable description of biophysical variables needed in simulating land surface fluxes.

A general, multi-dimensional approach with three or more bands, e.g., from Landsat or Sentinel-2, is beyond the scope of the current study. A multi-dimensional neural network approach was foreseen and promoted over 25 years ago by Baret et al. (1995). Note that dealing with more parameters in developing a sought relationship would imply potential instability of the parametric coefficients, in addition to the issue of collinearity. An approach for using multiple bands, as well as hyperspectral data, would be reduction in dimensionality using empirical orthogonal functions in principle component analysis (e.g. Ignatov and Gutman, 1999; Liu et al., 2017), with potential challenges in physical interpretation of the results.

In the current paper, however, we consider a simple species-specific, two-band parameterization for studying vegetation based on red and NIR observations alone. Therefore, this approach can ultimately be applicable to the development of global long-term time series of vegetation traits from the available archives of Advanced Very-High-Resolution Radiometer (AVHRR) data, which, in turn, would be useful to simulate long-term changes in the biosphere and surface fluxes during the past 40 years.

We start with an assumption that measured or modelled bio-physical variables, such as LAI, FPAR and Canopy Chlorophyll Content (CCC), can be parameterized statistically by a linear function of two explanatory remotely sensed variables: red and NIR observed reflectances, corrected for sun-target-sensor geometry and atmospheric effects. Commonly, LAI and FPAR empirical models have been developed based on derived relationships between LAI/FPAR and vegetation indices. For example, Fang and Liang (2008) reviewed models for estimating LAI and FPAR from optical remote sensing. Similarly, CCC estimations are based on its relationships with vegetation indices (e.g., Gitelson et al., 2005). When such vegetation index relationships are extrapolated to biomes or crops types beyond those that were used for developing such relationships, the accuracy of derived variables may decrease, unless the model is tuned to the new conditions. This provides challenge with vegetation index approach. Complex, non-linear vegetation indices are being developed for quantifying biosphere (e.g. Camps-Valls et al., 2021). The use of various linear and non-linear functions of reflectances has been also described by Miranda et al. (2020). A direct use of reflectances has been recently explored by Skakun et al. (2019); Skakun et al. (2021) in estimating crop yields.

In the current study, we propose a parameterization based on the weights (parameter coefficients) on the red and NIR reflectances that can be derived empirically from multiple linear regressions using in situ measurements of LAI, CCC and FPAR.[1] We hypothesize that these parameters are vegetation type-dependent but invariant in time and exhibit patterns over the globe, similar to those of vegetation classes. Ultimately, these weights can be tabulated and used for studying, modelling and global monitoring of vegetation, as well as parameterizing vegetation variables for various crops and forests in climate model simulations. Moreover, if a model grid contains various crops and/or forest types with the known fraction for each type, a parameterization for surface fluxes would use appropriate weights (coefficients) for subgrid fractions to estimate surface fluxes more accurately in a mixed model grid.

2. Background: two-band vegetation indices NDVI, RVI and DVI

There have been extensive overviews of available vegetation indices in the literature (e.g. Silleos et al., 2006). Therefore, we limit our background outlining only a few most popular two-band indices that have been widely used for deriving vegetation traits.

Among two-band vegetation indices, the Normalized Difference Vegetation Index (NDVI) has been one of the extensively used spectral

[1] An alternative way to obtain the sought coefficients would be by their "tuning" for the best correspondence of simulated fluxes in climate model runs with in situ measurements of those fluxes. However, other model parameters would introduce additional uncertainties.

indices for studying different vegetation traits from space due to its simplicity and robustness in land monitoring. It is still used in numerous vegetation-related applications as spatio-temporal dynamics of NDVI is well correlated with that of vegetation state. NDVI is calculated from remote sensing data as:

$$NDVI = \frac{\rho_2 - \rho_1}{\rho_2 + \rho_1}, \quad (1)$$

where ρ_2 and ρ_1 are NIR and visible (or red) reflectances, with band widths depending on a sensor varying from a wide 0.72–1.1 μm range in channel 2 (NIR) and 0.58–0.68 μm in channel 1 (visible) on Advanced Very-High-Resolution Radiometer (AVHRR) to a narrow range 0.85–0.88 μm for NIR and 0.64–0.67 μm for red reflectance on Landsat.

Eq. (1) can be also expressed through the Ratio Vegetation Index[2] (RVI) (Jordan, 1969; Pearson and Miller, 1972) $RVI = \frac{\rho_2}{\rho_1}$:

$$NDVI = \frac{RVI - 1}{RVI + 1} \quad (2)$$

RVI and NDVI are referred to by Broge and Leblanc (2001) as "angular indices", as they can be identified by the angle formed by the vector (with the origin in 0) in the Red-NIR bi-spectral space.

According to Broge and Leblanc (2001), these indices tend to enhance the contrast between soil and vegetation, minimize the effects of illumination conditions, and are sensitive to soil brightness effects, especially at low vegetation cover. In attempt to account for the background variability Huete (1988) introduced soil-adjusted vegetation indices that were later improved by transformation, adjustments and modifications (e.g., Baret et al., 1995; Qi et al., 1994).

The Difference Vegetation Index (DVI) (Jordan, 1969; Richardson and Wiegand, 1977) is another simple index, which has also been widely used for studying vegetation properties along with the ratio-based indices. In contrast to the "angular indices", DVI belongs to the broad category of "orthogonal indices", representing the orthogonal distance from a point corresponding to canopy reflectance to the soil line in red-near-infrared space (Baret and Guyot, 1991). This group includes the perpendicular vegetation index (PVI; Richardson and Wiegand, 1977) and the weighted difference vegetation index (WDVI; Clevers, 1989), both expressed as NIR-red linear combinations that are reduced to DVI under specific conditions. For example, WDVI $= \rho_2 - C^* \rho_1$, where C is *RVI* for bare soil reflectances, is reduced to DVI when the near-IR and red reflectances of the bare soil are equal (*RVI*=1).

If DVI is expressed as:

$$DVI = \rho_2 - \rho_1 = \rho_1 (RVI - 1) \quad (3)$$

it is easily understood that if DVI is calculated using top-of-atmosphere measured reflectances it would be prone to the atmospheric/bidirectional effects due to the red reflectance in (3), unless they are corrected and normalized. In other words, even though some effects are partially compensated in *RVI*, the effects in ρ_1 would produce spurious variability in DVI due to atmospheric/bi-directional effects. In fact, this is the main reason, why the NOAA weekly composites in the Global Vegetation Index (GVI) dataset (e.g., Gutman, 1994; Goward et al., 1993) and the NASA 10-day composites in the Global Inventory Monitoring and Modeling System (GIMMS) (e.g., Los et al., 1994; Tucker et al., 2005), both based on daily global AVHRR observations, have been so different. Different compositing procedures produce opposite biases (Gutman, 1991) because the NOAA compositing procedure was based on taking the maximum of DVI, which is the function of both *RVI* and ρ_1 (Eq. (3)), whereas NASA GIMMS composites have always been calculated using maximum NDVI (Holben, 1986), which is a function of *RVI* alone (Eq. (2)). As a result, the NOAA GVI composite dataset has a strong bias in backscatter, whereas in the NASA composite datasets the bias in observations is often shifted to forward scatter (see Figs. 4 and 5 in Gutman, 1991).

In what follows, we show results of exploring a vegetation-specific two-band parameterization for three biophysical variables (LAI, CCC, and FPAR) based on empirical multiple linear regressions and simulations using the radiative transfer PROSAIL model. In most of the above indices, equal weights, usually taken as 1, on the red and NIR reflectances are assumed in their combinations. By running empirical regressions, we establish to what extent and in what instances this assumption may not be valid. Once these weights are validated, tabulated, and their stability is established, they can be prescribed as a function of crop and forest type in land surface fluxes parameterizations in climate model simulations.

3. Methodology and data

3.1. Linear representation

Let us assume that a biophysical variable *V* characterizing vegetation can be represented as a linear function of two reflectances — ρ_1 (red) and ρ_2 (NIR):

$$V = k_1 \rho_1 + k_2 \rho_2, \quad (4)$$

which is reduced to DVI formulation (3) if $k_1 = -1$ and $k_2 = 1$. We propose to derive vegetation-specific coefficients k_1 and k_2 from empirical relationships based on available information on *V*, ρ_1 and ρ_2. In this parameterization, reflectance units are in percent (from 0 to 100). Rather than using a non-linear formulation for variable *V* and non-linear combinations of reflectances, we start with a simple linear approximation (4). In case of LAI, it would imply using only the first term in Maclaurin series. For example, deriving LAI based on the WDVI, requires a prescribed combination of extinction and scattering coefficients and the asymptotic value of the WDVI, which are further used as input in the non-linear formulation of LAI (Clevers and Verhoeff, 1993).[3] Additional tests with crop-specific and non-crop-specific non-linear models showed that the results either present challenges in interpretation or yield significantly higher RMSE (non-crop specific model) as compared with the proposed linear model. Potential further developments of the current model could include non-linearity.

Eq. (4) can be represented in the NIR-red bi-spectral space with

$$\rho_2 = V/k_2 - k_1/k_2 \rho_1, \quad (5)$$

which describes the family of lines $\rho_2 = a\rho_1 + b$ with a slope $a = -k_1/k_2$ and intercept $b = V/k_2$. The partial derivative $\frac{\partial \rho_2}{\partial V} = 1/k_2$ represents the rate of ρ_2 changes with *V* under fixed ρ_1. It should be noted that this rate, as well as slope *a*, do not depend on *V* itself, because the model is linear, which makes it different from previous studies, e.g., Huete (1988), Kallel et al. (2007), where the slope and intercept of isolines change with *V* due to models' non-linearity. Unlike previous studies directed at deriving generic, vegetation-independent relationships (Verrelst et al., 2012), the present study aims at exploring coefficients k_1 and k_2 for specific vegetation types using both close-range and satellite remote sensing data.

[2] This index is often referred to as Simple Ratio (SR), but for consistency with other indices we denote it as RVI.

[3] The k_1, k_2 coefficients include both the plant extinction/scattering and soil effects implicitly. Deriving them empirically with in situ observations should account for these effects. Our results with PROSAIL simulations, described further, compared well with empirically derived k_1, k_2 weights, hence we didn't pursue developing a non-linear approach leaving it to further investigation and potential improvements.

3.2. Data used

In order to explore patterns and regularities in coefficients in Eq. (4) for several vegetation types, we used the following datasets:

- ground-based measurements of vegetation variables and close-range reflectance observations with hyperspectral radiometers (AmeriFlux Nebraska sites—subsection 3.2.1),
- combined data from ground-based measurements of vegetation variables and satellite-derived reflectances (AmeriFlux Nebraska sites with Landsat 8, Sentinel-2 and Planet data—subsection 3.2.2; Ukraine site with Landsat 8 data—subsection 3.2.3); locations of the sites are shown in Fig. 1,
- MODIS-derived vegetation variables and the associated reflectances (subsection 3.2.4),
- simulated data using the PROSAIL radiative transfer model (subsection 3.2.5).

3.2.1. AmeriFlux Nebraska sites: close-range sensing and in-situ biophysical data

The study used multiple datasets of two crop species (maize and soybean) acquired and used in several previous studies (e.g., Ciganda et al., 2009; Gitelson et al., 2005; Verma et al., 2005; Viña et al., 2011) over three sites, across different years and at scales ranging from individual leaves to entire fields. While there is some variation among datasets, the data collection techniques in all studies employed standard procedures described below.

Data collection campaigns were carried out during the growing seasons (from May to September) of 2002–2005 in three AmeriFlux sites (US-Ne1, US-Ne2, and US-Ne3), located near Mead, Nebraska, USA. Both equipped with a center-pivot irrigation system, site 1 was under maize continuously, while site 2 was under a maize-soybean rotation (with maize in odd and soybean in even years). Site 3 was also under a maize-soybean rotation but relied entirely on rainfall (Verma et al., 2005). In the current study, we used soybean data for 2002 and 2004 and maize data for 2003 and 2005.

Canopy reflectance was measured using two inter-calibrated Ocean Optics USB2000 radiometers. One radiometer was equipped with a 25° field-of-view optical fiber pointing downward to measure canopy upwelling radiance within a 4.5 m^2 sampling area, while the other was equipped with an optical fiber and a cosine diffuser pointing upward to measure downwelling irradiance. Percent canopy reflectance was calculated as the ratio of upwelling radiance to downwelling irradiance (Rundquist et al., 2004; Viña et al., 2011).

Green LAI was determined destructively from samples collected in six small plots (20 m × 20 m) established within each sampling site, representing major soil and crop production zones within each site (Verma et al., 2005). In the laboratory, green leaf samples were run through a LI-3100, Li-Cor area meter to calculate leaf area per plant. This area was then multiplied by the plant population (assessed in each plot) to obtain green leaf area index LAI_g for each of the six plots, which were then averaged to obtain a site-level LAI_g value (Viña et al., 2011).

The chlorophyll content ([Chl]) of leaves sampled (ear leaf in maize plants and the top-most fully expanded leaf in soybean plants) was measured destructively in the lab. This was conducted concurrently with spectral reflectance measurements of the same leaves using an Ocean Optics radiometer equipped with a leaf clip. Foliar reflectance measurements were used to calculate the Red Edge Chlorophyll Index related to the destructive measurements of leaf [Chl]. This relation was then used to estimate non-destructively leaf [Chl] that was multiplied by LAI_g to provide an estimate of canopy chlorophyll content (CCC) (Ciganda et al., 2009; Gitelson et al., 2005).

3.2.2. AmeriFlux Nebraska sites: Landsat 8, Sentinel-2 and Planet Lab data

Measurements of LAI for the Nebraska sites were also available for 2018 and 2019. We took advantage of available remote sensing data, namely Landsat 8, Sentinel-2 and Planet Lab Doves (Planet Team, 2017), over the sites. Cloud-free satellite imagery were acquired over Nebraska sites US-Ne1, US-Ne2, and US-Ne3 for 2018 and 2019 to match ground measurements of LAI. The protocol for measuring LAI in 2018–2019 was the same as the one described in subsection 3.2.1. For Landsat 8 and Sentinel-2, we used NASA's Harmonized Landsat-Sentinel-2 (HLS) product at 30-m spatial resolution (Claverie et al., 2018) with all necessary corrections in deriving surface reflectance. For Planet Lab (Dove-Classic and Dove-R at 3-m spatial resolution and close-to-nadir observations with viewing angle 2–3°), we used an atmospherically corrected product with estimated surface reflectance. Satellite-derived reflectance in red and NIR were averaged over the Nebraska sites for compatibility with ground-based LAI measurements.

3.2.3. Ukraine site: Landsat 8, Sentinel-2 and in-situ data

Ground measurements of LAI over Ukrainian Joint Experiment for Crop Assessment and Monitoring (JECAM) test site (Kussul et al., 2014; Shelestov et al., 2017) were collected within the Imagine-S project (http://www.fp7-imagines.eu/pages/services-and-products/ground-data.php) for 2013–2015 and followed the Validation of Land European Remote sensing Instruments (VALERI) protocol (Morisette et al., 2006). Measurements were performed for the elementary sampling units (ESUs) of 30 m × 30 m to match the spatial resolution of satellite imagery (Landsat). A pseudo-regular sampling was used within each ESU with 12–15 samples per ESU, so the variability inside the moderate resolution pixel (30 m) can be captured. Each sample consisted of a digital hemispherical photo (DHP), which was further processed using CAN-EYE software (https://www6.paca.inrae.fr/can-eye) to derive LAI (Weiss et al., 2004) and averaged within the corresponding ESU and subsequently over plots. Ground measurements of LAI were collected for major crops, such as winter wheat (20 samples), maize (53) and soybean (17), and matched in space and time to the Landsat 8 reflectance data from the HLS product (Claverie et al., 2018).

3.2.4. MODIS data

Ideally, one should use independently measured, preferably at close range, LAI and FPAR for various land covers over the globe. However, this would entail a huge task of compiling sporadically available information, not readily available and often not accessible. We use MODIS products to demonstrate how our approach can be applied on a global scale because of their easy access and applicability but realizing that the results obtained in the global analysis of these data are for illustration only, merely to give a direction for future research.

To produce maps of parameters k_1 and k_2 at regional to global scales we used MODIS red and NIR atmospherically corrected normalized reflectances from the MOD09A1 product (Vermote, 2015), and LAI and FPAR from the MCD15A2H product Collection 6 (Myneni et al., 2015). Both products are generated at 500-m spatial resolution at 8-day intervals. When using the MOD09A1 product, we masked out pixels, identified as cloud, shadow, cirrus adjacent to cloud, or snow/ice. To derive LAI and FPAR (Myneni et al., 2015) the MCD15A2H product uses red (648 nm) and NIR (858 nm) MODIS spectral bands and a lookup table (LUT), generated using a 3D radiative transfer equation and stratified by biomes (Knyazikhin et al., 1998). Obviously, in this case LAI and FPAR cannot be considered fully independent variables as compared to the Nebraska and Ukraine cases because MODIS-derived products were based on the associated MODIS red and NIR bands. Previous studies using ground measurements provided the MODIS LAI and FPAR product uncertainties, as ±0.66 and ± 0.15, respectively (Yan et al., 2016). In this paper, regressions and coefficients k_1 and k_2 were estimated for each 500-m pixel separately using red and NIR reflectances and LAI and FPAR throughout the whole year 2017. Areas, which had less than 5 8-day high-quality observations during the year, were marked as "No data".

Note that MODIS biome map includes a rather coarse classification of

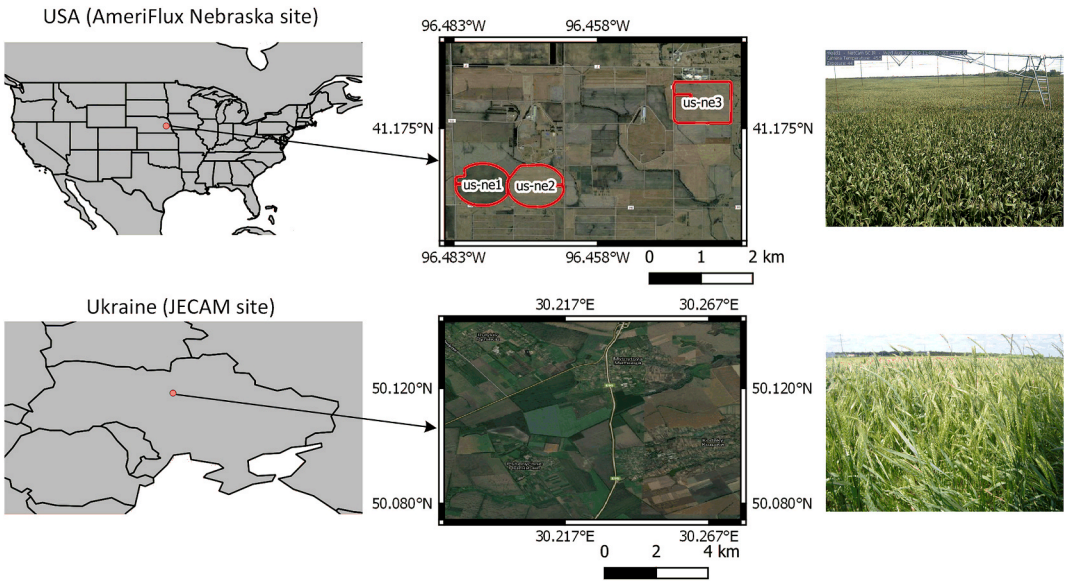

Fig. 1. Location of the sites.

croplands. To explore spatial patterns of k_1 and k_2 for specific crops and forest types in the continental USA we used a 30-m USDA Cropland Data Layer (CDL) map (Boryan et al., 2011; Johnson and Mueller, 2010) and a 250-m forest type map of USDA's Forest Service.[4] We calculated proportions of 30-m pixels with specific crops in 500-m pixels. Regression analysis for specific crops was performed only for 500-m pixels with the 100% purity. The same procedure was performed for the 250-m forest type map.

3.2.5. PROSAIL model simulations

In search of the optimal k_1 and k_2 coefficients in multiple linear regression analysis, we used PROSAIL model (version 5B) (Feret et al., 2008; Jacquemoud et al., 2009; Verhoef, 1984) to simulate red ρ_1 (0.67 μm) and NIR ρ_2 (0.8 μm) reflectances for three crops – soybean, maize and rice - based on various input parameters, including LAI and leaf chlorophyll content. PROSAIL is a radiative transfer model, which simulates canopy spectra based on the following inputs: plant leaf properties (chlorophyll, carotenoid and brown pigment contents, dry matter, water content, structure); dry/wet soil; and canopy properties (LAI, hot spot, solar and observing angles). Overall, 100 spectra were generated with the range of input parameters for these crops following Inoue et al. (2016) and Gitelson et al. (2021) (Table 1). We used the Latin Hypercube sampling to sample input variables (Verrelst et al., 2016). Following Jacquemoud et al. (2009), the sun-target-sensor geometry was fixed at solar zenith angle 30°, with the observer zenith and azimuth angles equal to 0°.

3.3. Analysis design

Ground-based measurements at Nebraska sites (subsection 3.2.1) were used to establish coefficients k_1 and k_2 for maize and soybean. To test robustness and stability of those coefficients, we ran regressions for individual years as well as leave-one-out cross-validation (LOOCV). Performance of established relationships was measured in terms of the root mean square error (RMSE), relative RMSE (RRMSE) and the coefficient of determination (R^2>):

$$RMSE = \sqrt{{}^1\!/\!_n \sum_{i=1}^{n} \left(V_{est} - V_{ref}\right)^2},$$

$$RRMSE = 100\% \times RMSE \Big/ \overline{V}_{ref},$$

$$R^2 = 1 - \frac{\sum_{i=1}^{n} \left(V_{est} - V_{ref}\right)^2}{\sum_{i=1}^{n} \left(\overline{V}_{ref} - V_{ref}\right)^2}$$

where V_{est} and V_{ref} are estimate and reference values, respectively; $\overline{V}_{ref} = {}^1\!/\!_n \sum_{i=1}^{n} V_{ref}$ is the average of the reference values, and n is the number of samples.

For comparisons with other indices (NDVI) and non-linear models, we also used a noise equivalent (NE) metric (Gitelson, 2013) that provides a measure of how well the VI responds to biophysical parameters across its entire range of values (dynamic range):

$$\text{NE } \Delta V = \text{RMSE } (VI \text{ vs. } V) \,/\, [\mathrm{d}(VI)/\mathrm{d}(V)]$$

In order to assess variability of biophysical variables, we used coefficient of variation (Cov):

$$Cov = 100\% \times \frac{\sigma_V}{\mu_V}$$

where σ_V and μ_V are the standard deviation and the mean of variable V.

We used coefficients k_1 and k_2 (derived from the ground data in subsection 3.2.1) and directly applied them to satellite-derived reflectances in Nebraska (HLS and Planet Lab, subsection 3.2.2) and Ukraine (HLS, subsection 3.2.3) to estimate biophysical traits. We then validated the derived variables against ground-based measurements of CCC, LAI and FPAR, whatever was available. Using the maps of coefficients k_1 and k_2 derived from MODIS at 500-m spatial resolution (for LAI and FPAR) and the CDL map (subsection 3.2.4), we analyzed MODIS-derived patterns of the coefficients globally as well as compared them to those derived from the Nebraska dataset for the two crops.

4. Results

4.1. Comparison of PROSAIL simulations with results from ground observations

The coefficients k_1 and k_2 are derived from multiple regressions of LAI, CCC and FPAR against red and NIR reflectances obtained at the

[4] https://data.fs.usda.gov/geodata/rastergateway/forest_type/index.php.

Table 1
LIDF is the Leaf Inclination Distribution Function; N is the leaf structure parameter; Cab is the leaf chlorophyll content; Car is the carotenoid content; Cbr is the brown pigment fraction; Cw is the water content; C*m* is the dry matter content; and LAI is the green leaf-area index.

CROP	LIDF	N	Cab, μg cm^{-2}	Car, μg cm^{-2}	Cbr	Cw, cm	C*m*,g cm^{-2}	LAI
Maize	LIDFa = 70 LIDFb = 0	1.4–1.8	30–60	8–15	0–0.1	0.01–0.03	0.001	0.2–5.6
Soybean	Planophile	1.1–1.5	30–60	8–15	0–0.1	0.001–0.03	0.00075	0.2–5.6
Rice	Erectophile	1–2	20–40	5–10	0–0.1	0.001–0.03	0.0005–0.0015	0.2–6.5

Nebraska sites and in simulations using PROSAIL model (Table 2). The standard deviations for k_1 and k_2 coefficients (Table 2) are within 5–10% of the mean values. We did not run FPAR retrievals from PROSAIL for technical reasons. Ground observations for rice have not been provided to this study, hence the comparison is only made between PROSAIL- and MODIS-derived coefficients.

The coefficients derived from empirical data do not differ from the corresponding PROSAIL coefficients by more than the corresponding standard deviations except for soybean LAI k_1 and maize CCC k_1. For both LAI and CCC, the k_1 and k_2 values derived at Nebraska site for maize are substantially higher than those for soybean. For FPAR, the k_1 and k_2 absolute values are practically identical for both crops (−0.02 and 0.02 for the k_1 and k_2, respectively).

Fig. 2 shows dependence of CCC on NIR for a small range of red reflectance values as derived from Eq (4) using ground-based k_1 and k_2 in Table 2:

maize: $CCC = -0.13\,\rho_1 + 0.07\rho_2$,

soybean: $CCC = -0.06\,\rho_1 + 0.03\rho_2$.

The derived coefficients imply that for the same observed reflectances of the two crops the chlorophyll content of maize is double of that of soybean, which is illustrated in Fig. 2. It agrees quantitatively with the empirical and PROSAIL-simulated relationships of absorption coefficient with CCC in maize and soybean canopy (Gitelson et al., 2019). They explained their finding by the differences in leaf absorption coefficients at 0.67 μm and leaf areas between these two crops.

The main distinction between the soybean and maize is by their division into two groups — C3 (soybean) and C4 (maize) — depending on how they convert light energy into sugar or photosynthesize. C3 crops have a unique leaf anatomy allowing carbon dioxide to concentrate in bundle sheath cells; C4 crops do not have this anatomic structure, so that C4 pathway implies that resources are processed more efficiently and converted into higher grain production. For the same canopy chlorophyll content, the larger soybean leaf area is responsible for a more effective absorption by the soybean canopy. The proposed method, therefore, provides species-specific parameters for estimating CCC— an important structural and biochemical trait of vegetation.

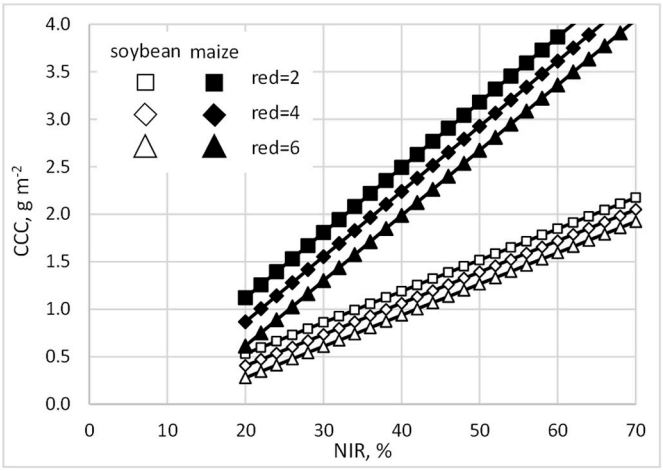

Fig. 2. Canopy chlorophyll content (CCC) as a function of NIR reflectance for three red reflectance values at the Nebraska sites.

To test the stability of the coefficients k_1 and k_2 from year to year we ran regressions separately for each year for all available data in Nebraska. Table 3 indicates that year-to-year variations of coefficients are within the standard errors suggesting a relative temporal stability of crop-specific k_1 and k_2.

4.2. *Leave-one-out cross-validation of the maize and soybean parameterizations at Nebraska site*

Uncertainties of crop-specific coefficients k_1 and k_2 retrievals (Table 2) for LAI and CCC estimation were tested using LOOCV methodology (Fig. 3). The RMSE does not exceed 0.57 for LAI, 0.35 for CCC, and 0.11 for FPAR (Table 4).

These results (along with the ones from Table 2) show that the

Table 2
Coefficients k_1 and k_2 from multiple linear regression using reflectances observed at the ground at Nebraska sites (left) and simulated with PROSAIL model (right).

Variable	Crop	Ground-based (Nebraska sites)			PROSAIL		
		k_1	k_2	R^2	k_1	k_2	R^2
LAI	Maize	−0.19 ± 0.014	0.11 ± 0.006	0.90	−0.18 ± 0.010	0.10 ± 0.005	0.93
LAI	Soybean	−0.12 ± 0.014	0.08 ± 0.006	0.85	−0.17 ± 0.014	0.08 ± 0.006	0.89
LAI	Rice	–	–	–	−0.25 ± 0.014	0.13 ± 0.001	0.97
CCC	Maize	−0.13 ± 0.010	0.07 ± 0.004	0.89	−0.11 ± 0.007	0.06 ± 0.004	0.90
CCC	Soybean	−0.06 ± 0.010	0.03 ± 0.004	0.77	−0.07 ± 0.007	0.04 ± 0.003	0.84
CCC	Rice	–	–	–	−0.09 ± 0.010	0.04 ± 0.003	0.85
FPAR	Maize	−0.02 ± 0.003	0.02 ± 0.001	0.86	–	–	–
FPAR	Soybean	−0.02 ± 0.003	0.02 ± 0.001	0.79	–	–	–

Table 3
Coefficients k_1 and k_2 derived for maize and soybean using ground measurements from Nebraska for different years.

Crop	Years	LAI		CCC	
		k_1	k_2	k_1	k_2
Maize	All years	−0.19 ± 0.01	0.11 ± 0.006	−0.13 ± 0.01	0.07 ± 0.004
Maize	2003	−0.18 ± 0.02	0.11 ± 0.006	−0.12 ± 0.01	0.07 ± 0.004
Maize	2005	−0.19 ± 0.02	0.12 ± 0.006	−0.14 ± 0.01	0.07 ± 0.004
Soybean	All years	−0.12 ± 0.01	0.08 ± 0.006	−0.06 ± 0.01	0.03 ± 0.004
Soybean	2002	−0.12 ± 0.01	0.08 ± 0.006	−0.06 ± 0.01	0.03 ± 0.004
Soybean	2004	−0.13 ± 0.03	0.07 ± 0.006	−0.07 ± 0.01	0.03 ± 0.004

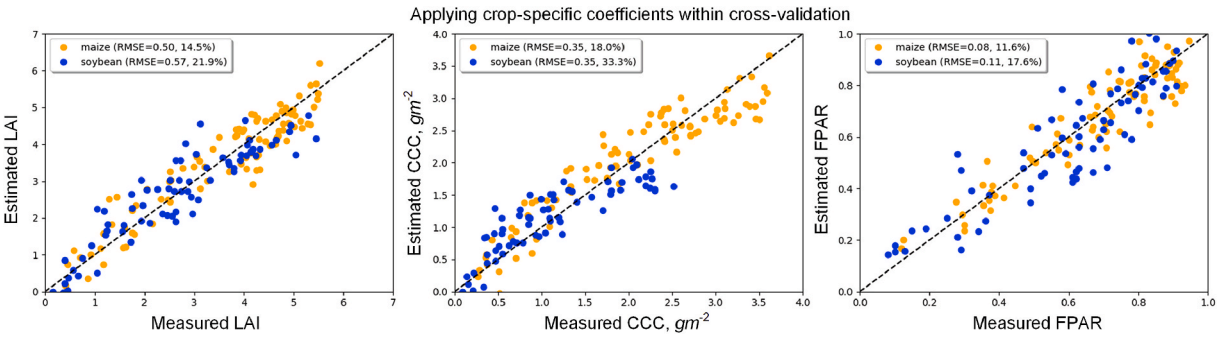

Fig. 3. Estimated vs. measured LAI, CCC and FPAR, when applying crop-specific coefficients k_1 and k_2 estimated through leave-one-out cross-validation using data at the Nebraska sites.

Table 4
Results of leave-one-out cross-validation of LAI, CCC, and FPAR retrievals from close-range measured reflectances at the Nebraska sites.

Variable	Crop	Ground-based		
		RMSE	RRMSE, %	R^2
LAI	Maize	0.50	14.5	0.9
LAI	Soybean	0.57	21.9	0.84
CCC	Maize	0.35	18	0.88
CCC	Soybean	0.35	33.3	0.76
FPAR	Maize	0.08	11.6	0.85
FPAR	Soybean	0.11	17.6	0.78

suggested model (Eq. (4)) is adequate and robust enough for accurate estimation of biophysical parameters using reflectances in red and NIR spectral bands. RMSE values (Table 4) are at the level or better than those obtained in previous studies utilizing vegetation indices, multiple spectral bands and machine learning methods (Kang et al., 2016; Nguy-Robertson and Gitelson, 2015; Verrelst et al., 2016).

We also compared our linear approach with adaptive weights to two other indices: DVI (Eq. (3)) and NDVI (Eq. (2)). For DVI, we used a linear model, while for NDVI a non-linear exponential model was applied. The results are presented in Table 5.

While the RMSE values are lower for the NDVI model, the NE is higher for LAI and CCC, because of the NDVI saturation occurring at high LAI values, which is a well-known problem with NDVI. High NE values for LAI and CCC means that NDVI is not sensitive to changes in LAI/CCC values. The current model also yielded better metrics (RMSE and NE) compared to DVI with fixed weights. For FPAR, performance of all three approaches (Table 5) is the same.

4.3. Model performance for moderate- (HLS 30 m) and very high-resolution (Planet Lab Doves 3 m) data

Time series of ground-based measurements of LAI along with LAI derived from HLS (Landsat and Sentinel-2) and Planet Lab (Doves) data using k_1 and k_2 coefficients from Table 2 are shown in Fig. 4 and the corresponding plots of estimated LAI versus measured LAI are shown in Fig. 5. Temporal profiles of the satellite-derived LAI values follow closely the ground-based LAI measurements (Fig. 5). RMSE values of maize LAI estimation were 0.63 (bias of 0.01) and 0.61 (−0.12) for HLS and Planet, respectively; RMSE for soybean was 0.60 (bias of −0.15) and 0.58 (−0.32) for HLS and Planet, respectively. RMSE values were slightly higher than RMSE of LAI estimation based on close-range reflectance measurements (Table 4).

A slight underestimation of both HLS- and Planet-derived values at high LAI as compared to ground measurements can be observed in Figs. 4 and 5. Negative bias was larger for soybean, than for maize. Preliminary analysis suggests that both HLS and Planet NIR reflectance observations reach saturation for high LAI values (greater than 5), whereas red reflectance values in both HLS and Planet data also saturate (to around 2%) at LAI around 4. These effects are not visible for ground-observed reflectances and PROSAIL simulations, thus the resulting biases may be attributable to some residual atmospheric correction errors, but this needs to be further investigated.

No bandpass adjustments were done as the level of uncertainties in spectral bandpass adjustments is lower than uncertainties associated with biophysical properties retrievals. Additional comparisons (not included here) of estimated coefficients using Planet-derived reflectances with those derived with in situ data and PROSAIL simulations showed that all coefficients are within their standard errors, indicating that bandpass adjustments' influence would be minimal.

Table 5
Comparison of various models for LAI, CCC and FPAR using calibration data at the Nebraska sites. For LAI and CCC, a non-linear NDVI model (exponential) was used, while for FPAR a linear model was used.

Variable	Crop	Current model		DVI		NDVI	
		RMSE	NE	RMSE	NE	RMSE	NE
LAI	Maize	0.49	0.51	0.53	0.57	0.39	0.46 to 1.34
LAI	Soybean	0.55	0.60	0.58	0.63	0.52	0.47 to 1.69
CCC	Maize	0.35	0.37	0.34	0.36	0.32	0.38 to 1.02
CCC	Soybean	0.34	0.39	0.34	0.39	0.31	0.30 to 0.88
FPAR	Maize	0.08	0.08	0.08	0.08	0.07	0.08
FPAR	Soybean	0.10	0.11	0.10	0.11	0.07	0.08

4.4. Validation with data at the Ukrainian site

When coefficients k_1 and k_2 generated using data obtained at Nebraska sites (Table 2) were directly applied to red and NIR reflectances from HLS (Landsat-8) over the Ukrainian site and compared to LAI ground measurements, the RMSE values for maize and soybean LAI were 0.51 and 0.53, respectively (Fig. 6), consistent with those derived for Nebraska with HLS data. Moreover, the performance of the Nebraska-calibrated model at the Ukrainian site is similar to that of the models, which were calibrated using Ukrainian data (Shelestov et al., 2017). This suggests that coefficients from Table 2 can be applicable for similar cropping systems in different geographic locations.

We also assessed the regression coefficients for specific crops (maize, soybean and wheat) in LAI estimation using directly Ukrainian data (Table 6). The derived coefficients for maize and soybean are close to those derived using Nebraska data and PROSAIL simulations (Table 2). It is encouraging to see their robustness, when applied to a different region.

4.5. MODIS LAI and FPAR products

In this section, we illustrate the proposed approach on a regional

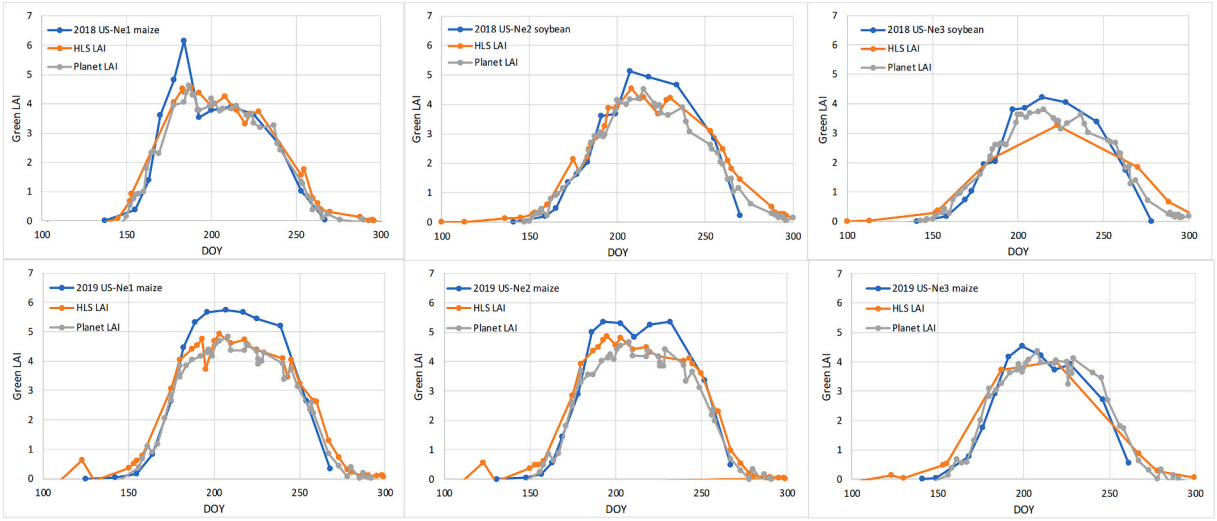

Fig. 4. Time series of ground-based LAI and LAI derived from satellite data (HLS and Planet) for the three fields in Nebraska (2018–2019).

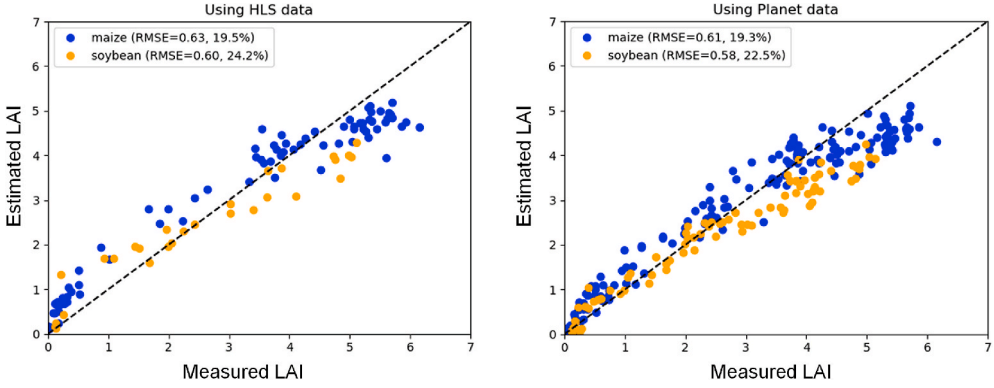

Fig. 5. Estimated LAI (from HLS and Planet data using the proposed parameterization) vs. measured LAI at the three fields in Nebraska sites (2018–2019).

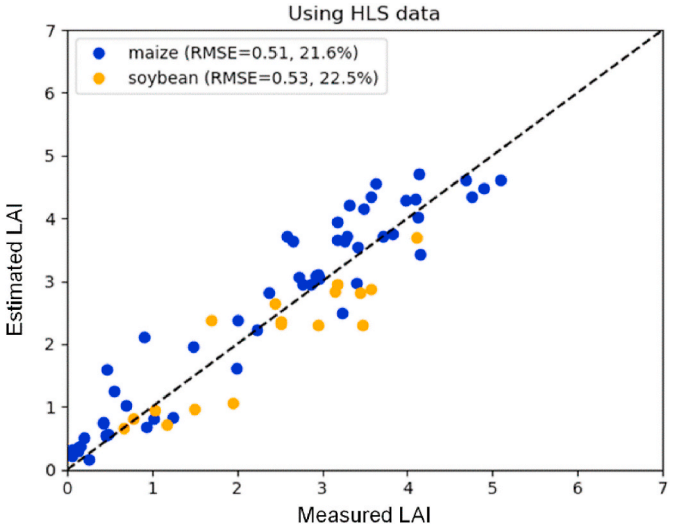

Fig. 6. Estimated LAI (from HLS) vs. reference LAI (from ground-based measurements) for maize and soybean fields in Ukraine (2013–2015).

(CONUS) to global scale. As mentioned earlier, the MODIS products are dependent on observed reflectances, hence the preliminary results in what follows are for demonstrating purposes only, indicating some interesting features. The derived coefficients are definitely premature for applying in large scale mapping and modeling. However, it was encouraging to see that the MODIS-derived coefficients for maize and soybean areas corresponded pretty well to those derived using independent LAI and FPAR measurements in Nebraska sites. We stress that independent measurements over various vegetation types should be compiled to develop a reliable set of coefficients that can be tabulated for further use in land surface parameterizations on a large scale.

4.5.1. *MODIS LAI and FPAR analysis for specific crops in the conterminous USA*

Fig. 7 shows distribution of several major crops (maize, soybean, winter wheat and rice) in the continental U.S. (CONUS) derived from USDA CDL, and Fig. 8 shows the histograms of k_1 and k_2 derived for these cropland classes using regressions on MODIS LAI and FPAR. The corresponding averaged values and their standard deviations are provided in Table 7.

For LAI, all crops (except rice) feature a single peak with values of k_2 between 0.08 and 0.09 (with standard deviations of about 0.02), corresponding specifically to the soybean LAI ground-based model and supported by PROSAIL simulations (Table 2). It can be explained by the fact that the MODIS-based LAI model (used in MCD15) does not account for specific crop types, i.e., a generic model for all crops was used by MODIS product developers. What is interesting in Fig. 8 is that the histogram of LAI coefficients for rice (red line) is bimodal, exhibiting two peaks for both k_1 and k_2. We explored the geographic distribution of rice crops over the U.S. and discovered two clear patterns corresponding to two major rice-producing regions in the U.S.: California and Arkansas

Table 6
Results of applying the linear model Eq. (4) for LAI using Ukrainian data only.

Crop	k_1	k_2	Calibration			Cross-validation		
			RMSE	RRMSE, %	R^2	RMSE	RRMSE, %	R^2
Maize	−0.21 ± 0.03	0.11 ± 0.004	0.45	19.0	0.91	0.46	19.4	0.91
Soybean	−0.12 ± 0.03	0.08 ± 0.009	0.44	18.7	0.92	0.47	19.9	0.80
Wheat	−0.35 ± 0.05	0.12 ± 0.006	0.51	22.8	0.90	0.58	25.9	0.87

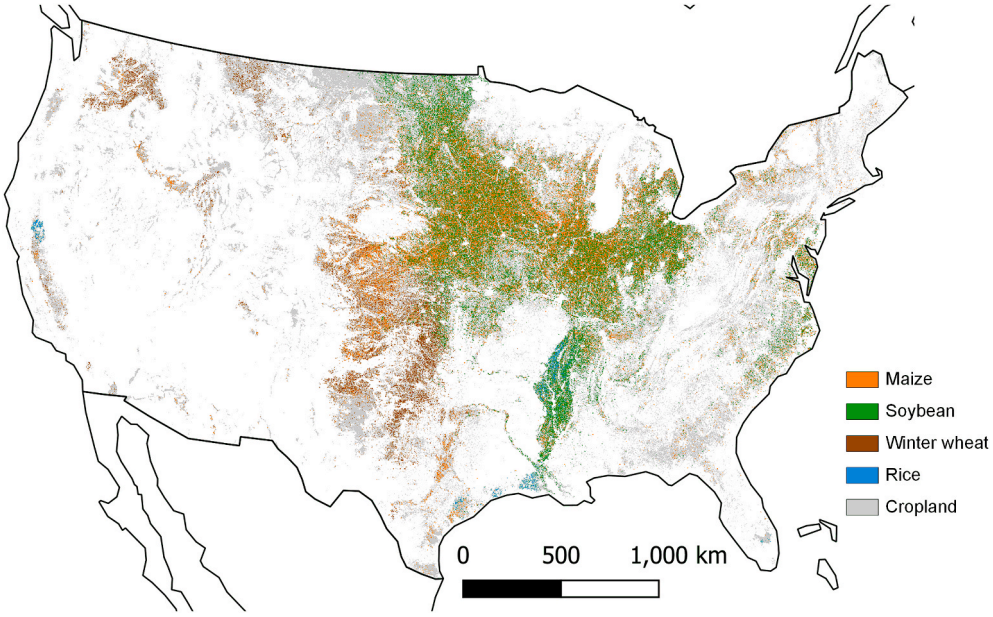

Fig. 7. Distribution of cropland and major crops (maize, soybean, winter wheat and rice) in the CONUS in 2017 based on the Cropland Data Layer (USDA) map.

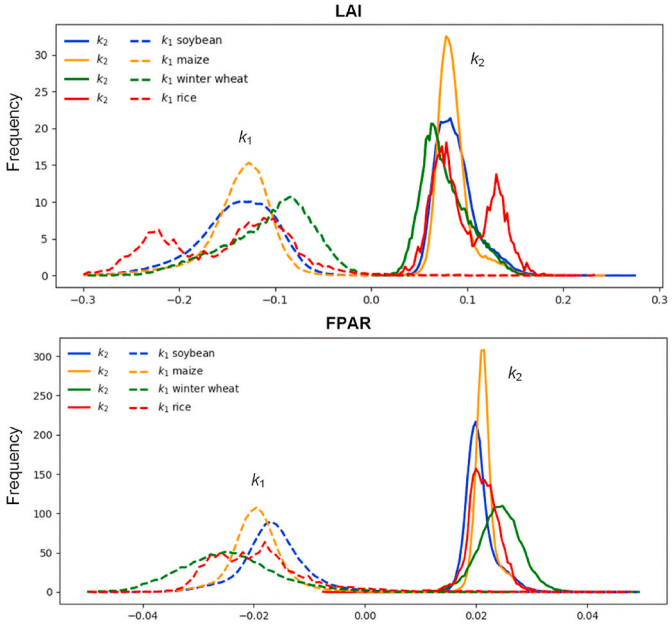

Fig. 8. Distribution of k_1 and k_2 for four crop types, derived for LAI (top) and FPAR (bottom).

(Fig. 9).

Fitting this bimodal distribution with a Gaussian mixture model with two components yielded two separate sets of k_1 and k_2 values: 0.12 and 0.08 for Arkansas (AR); and -0.23 and k_2 = 0.13 for California (CA).

Table 7
Coefficients k_1 and k_2 derived from correlations of MODIS LAI and FPAR with MODIS reflectances in red and NIR bands for specific crops in the CONUS.

Variable	Crop	k_1	k_2	$-k_1/k_2$
LAI	Maize	−0.13 ± 0.03	0.09 ± 0.02	1.5 ± 0.5
LAI	Soybean	−0.14 ± 0.04	0.09 ± 0.02	1.5 ± 0.6
LAI	Rice (AR)	−0.12 ± 0.05	0.08 ± 0.02	1.5 ± 0.4
LAI	Rice (CA)	−0.23 ± 0.02	0.13 ± 0.01	1.8 ± 0.2
LAI	Winter wheat	−0.10 ± 0.05	0.08 ± 0.02	1.3 ± 0.7
FPAR	Maize	−0.02 ± 0.005	0.02 ± 0.002	0.9 ± 0.2
FPAR	Soybean	−0.02 ± 0.01	0.02 ± 0.003	0.8 ± 0.2
FPAR	Rice (AR, CA)	−0.02 ± 0.01	0.02 ± 0.003	0.9 ± 0.2
FPAR	Winter wheat	−0.02 ± 0.01	0.02 ± 0.004	1.0 ± 0.2

Preliminary results with ground observations indicate that the derived values for California, with predominant Japonica rice (short- or medium-grain), correspond to rice in Japan, while the values for Arkansas with predominant Wells type rice (long-grain) are similar to the values for soybean, which reiterates the importance of developing crop-specific relationships for LAI (see Fang and Liang, 2008).

The k_1 and k_2 coefficients derived from MODIS LAI and FPAR regressions against reflectances are summarized in Table 7.

4.5. 2 MODIS LAI and FPAR analysis for specific forest types in the U.S.

Fig. 10 shows the geographic distribution of forest types over CONUS derived from USDA's Forest Service dataset. We used cluster analysis to reduce the number of sub-classes for both evergreen and deciduous forest classes. Table 8 shows the grouping of the forest type sub-classes. In deriving the regression coefficients, we relied on the MODIS LAI and FPAR products (as independent variable), so one should bear in mind

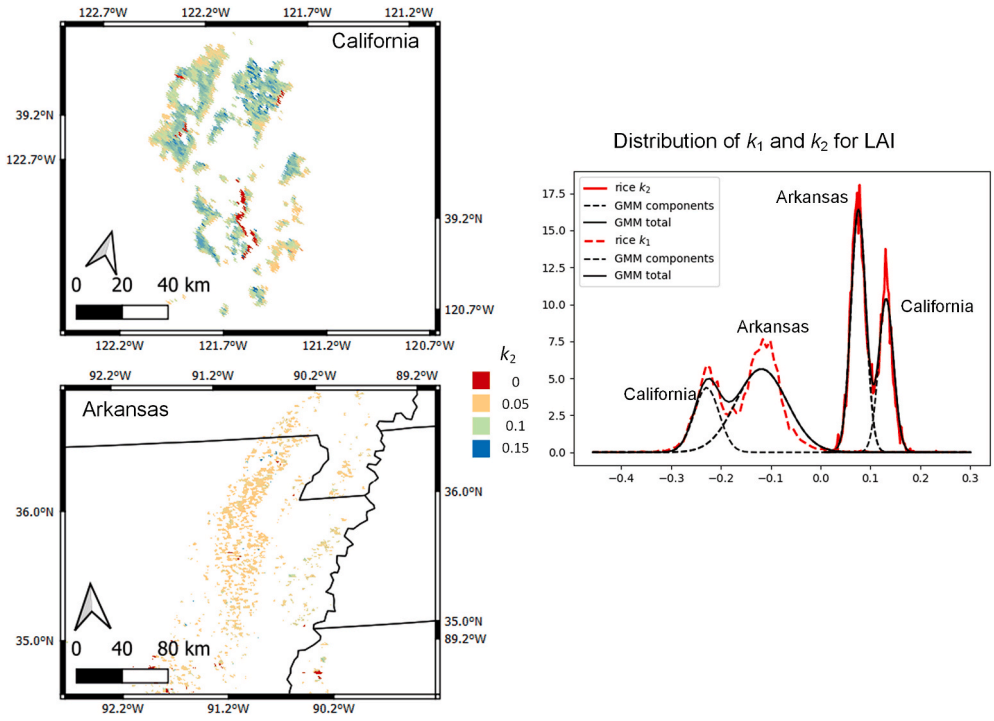

Fig. 9. The two geographical areas corresponding to the two modes in k_2 derived for LAI for rice (left) and the histograms of k_1 and k_2 values, where two modes are fitted with Gaussian mixture model with two components (right).

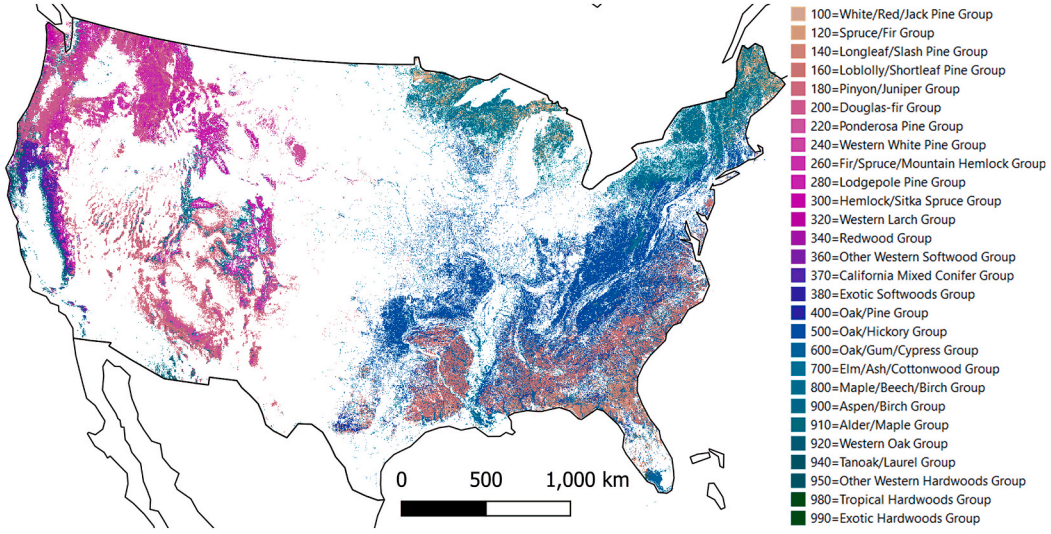

Fig. 10. Forest type map for CONUS.

that associated uncertainties would propagate in our regression results. Table 9 shows associated k_1 and k_2 derived from LAI and FPAR regressions.

Most LAI histograms for both evergreen and deciduous sub-classes have reasonably narrow distributions for k_2 between 0.1 and 0.2, and much wider for k_1 for some of the sub-classes (sub-class 3 for evergreen and sub-class 2 for deciduous). The histogram distributions of k_2 for both the evergreen sub-class 3 and deciduous sub-class 2 shift towards 0.2 and have no distinct peak for k_1. In Table 9, only some k_1 values for FPAR are close to those for crops but some substantially different with large standard deviation. The k_2 values are all 2–3 times higher than those for crops with a reasonably small variance. This suggests that while a simple difference index, DVI, could be a good proxy in estimating FPAR for some crops, as the values of k_1 and k_2 are close, this may not be appropriate for forests, where 1.5-3 times higher weights on NIR should be used in combinations of red and NIR reflectances. Future investigations with LAI and FPAR in-situ observations for forests will be needed to verify this preliminary conclusion.

The results from Fig. 11Fig. 10 and Table 8 suggest that the uncertainty in LAI estimates using the current model could be large due to the uncertainty in k_1. But for at least a couple of evergreen sub-classes and a couple of deciduous sub-classes the LAI estimates should be reasonably good. However, much more research using in situ LAI/FPAR measurements in forests would be required to develop a set of coefficients for practical applications in models.

4.5.3. *MODIS LAI and FPAR global analysis*

In this section, we show results of applying our proposed

Table 8
Forest type groupings based on k_2 and k_1 derived for LAI. For sub-classes 3, percentages of each special type in that group are indicated.

Evergreen		Deciduous	
Sub-class	Forest type	Sub-class	Forest type
1	Pinyon/Juniper	1	Oak/Pine, Western Oak
2	Ponderosa Pine	2	Tanoak/Laurel
3	Lodgepole Pine (6%), White/Red/Jack Pine (1%), Spruce/Fir (7%), Longleaf/Slash Pine (9%), Loblolly/Shortleaf Pine (30%), Douglas-fir (26%), Fir/Spruce/Mountain Hemlock (13%), Hemlock/Sitka Spruce (1%), California Mixed Conifer (7%)	3	Oak/Gum/Cypress (6%), Elm/Ash/Cottonwood (1%), Oak/Hickory (62%), Maple/Beech/Birch (25%), Aspen/Birch (6%)

Table 9
Coefficients k_1 and k_2 derived for forest sub-classes (Table 8) from correlations of MODIS LAI and FPAR with MODIS reflectances in red and NIR bands.

Variable	Sub-class	k_1	k_2
LAI	Evergreen Sub-class 1	-0.12 ± 0.06	0.08 ± 0.03
LAI	Evergreen Sub-class 2	-0.22 ± 0.12	0.14 ± 0.05
LAI	Evergreen Sub-class 3	-0.30 ± 0.15	0.20 ± 0.06
LAI	Deciduous Sub-class 1	-0.24 ± 0.14	0.14 ± 0.06
LAI	Deciduous Sub-class 2	-0.30 ± 0.17	0.20 ± 0.08
LAI	Deciduous Sub-class 3	-0.33 ± 0.11	0.17 ± 0.03
FPAR	Evergreen Sub-class 1	-0.02 ± 0.02	0.03 ± 0.01
FPAR	Evergreen Sub-class 2	-0.02 ± 0.02	0.04 ± 0.01
FPAR	Evergreen Sub-class 3	-0.01 ± 0.02	0.03 ± 0.01
FPAR	Deciduous Sub-class 1	-0.02 ± 0.02	0.03 ± 0.01
FPAR	Deciduous Sub-class 2	0.01 ± 0.03	0.03 ± 0.01
FPAR	Deciduous Sub-class 3	0.002 ± 0.01	0.03 ± 0.01

parameterization using MODIS data globally, with caveats noted in the beginning of section 4.5. Fig. 12 shows the global distribution of the land-cover classes used in the MODIS LAI/FPAR products (Knyazikhin et al., 1998) (top) and that of coefficient k_2 (bottom), derived for each map cell at 500-m spatial resolution using regressions of MODIS LAI (MCD15) data on the corresponding red and NIR normalized reflectances (MOD09).

Fig. 12 shows distinct spatial patterns corresponding to different land-cover classes and corresponds qualitatively rather well to the biome distribution. Since the MCD15 product uses biome-specific look-up tables (Knyazikhin et al., 1998; Myneni et al., 2015), the regression coefficients are expected to differ for the 8 biomes, but the regularity of the patterns is rather remarkable taking into account that the coefficients were obtained for each map cell independently. It is important to note that LAI is a vegetation *state* variable while we postulated a set of coefficients k_1 and k_2 to be an *inherent characteristic* of a land-cover class (or sub-class). If it was not the case the resulting map would be noisy presenting no regular patterns.

Fig. 13 shows histograms of k_1 and k_2 for LAI and FPAR for the eight MCD15 biomes (Fig. 12 top). The LAI histograms for generalized crops have reasonably narrow distributions for k_2 around 0.1 and k_1 around -0.1. The distributions of k_2 and k_1 for savanna (a mix of grassland with trees) LAI are shifted to larger absolute values, and for forest classes the shift is even further. The widespread in k_1 histograms indicates a potential need for finer stratification for sub-classes, as was analyzed in the previous section. It also indicates at the limitation of the proposed parameterization in some regions. For example, the B5 biome (evergreen broadleaf forest) in Fig. 12 (top) represents tropical rainforest areas with low annual variability, where a regression approach fails, as will be discussed below. Note that the results for the globe are for demonstration purposes only and should be considered qualitative and preliminary merely to outline the common features and trends.

To identify regions of applicability of the proposed model, we present in Fig. 14 (top) the global distribution of LAI Cov derived from the MCD15A2H product for 2017. The areas with low Cov values are mainly arid regions and rainforest areas, both characterized by low annual variability, where regression analysis produces spurious results (with

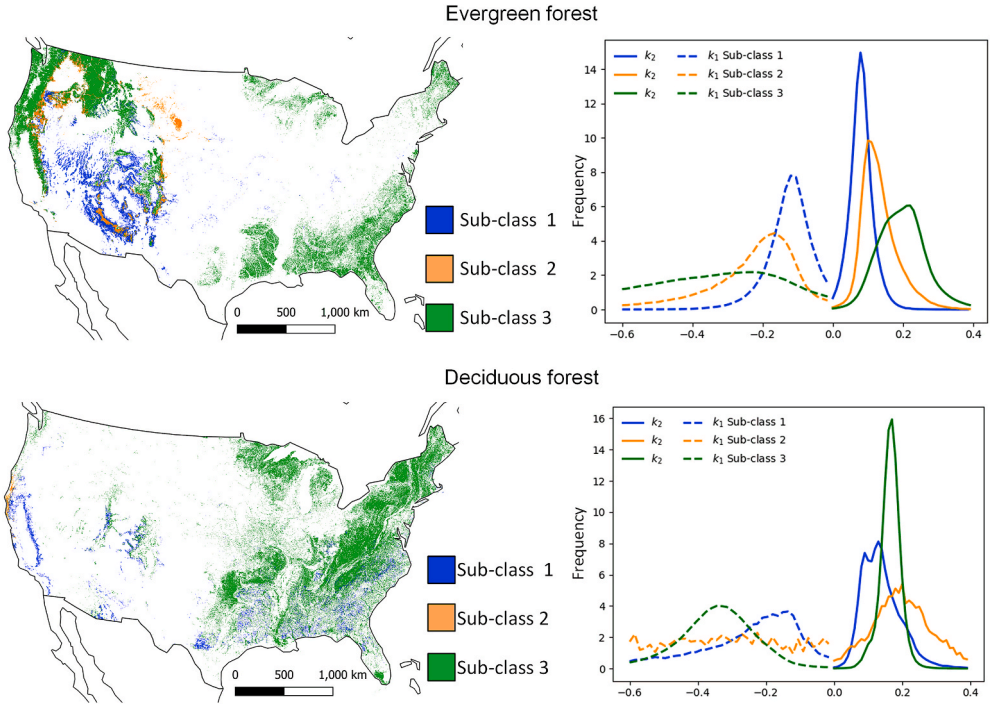

Fig. 11. The geographic distribution of evergreen (top) and deciduous (bottom) forest sub-classes (left panel) and their corresponding histograms (right panel). Forest types included in each sub-class are provided in Table 8.

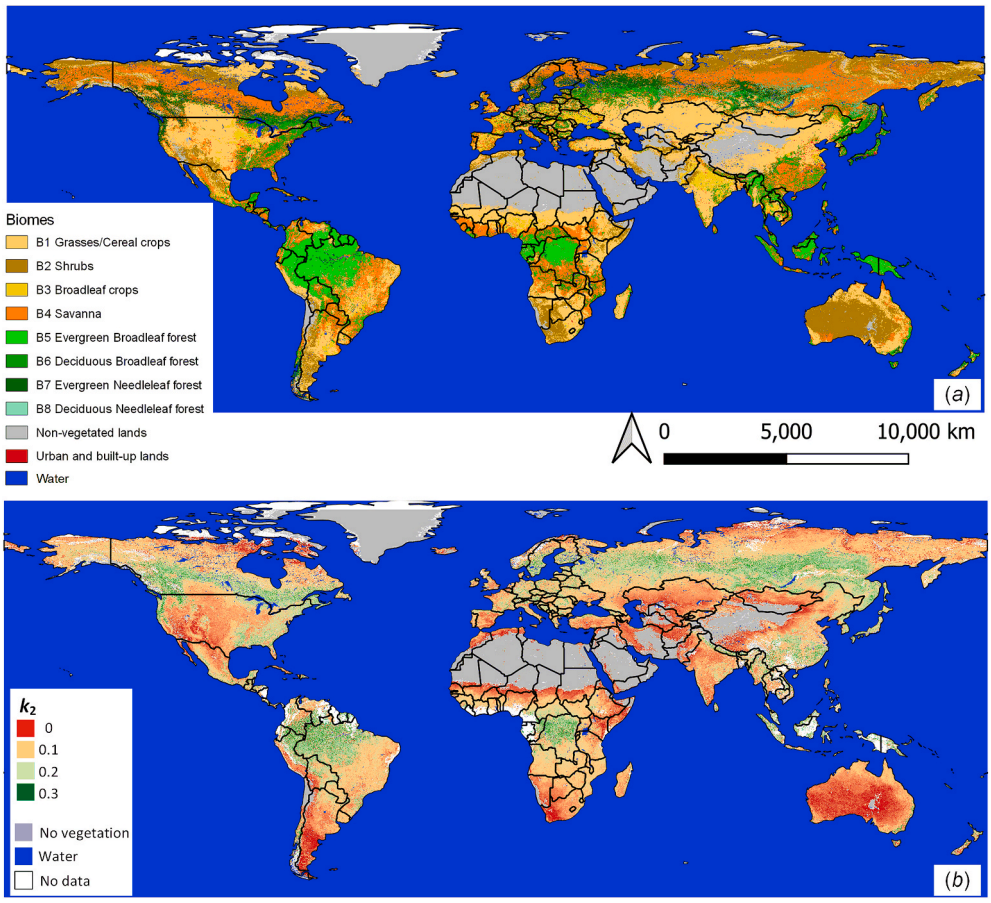

Fig. 12. Geographic distribution of biomes used in the production of the LAI/FPAR MCD15A2H product (top) and of k_2 derived from LAI regressions with using MODIS product in 2017 (bottom). "No data" indicate areas, where not enough satellite measurements were available because of cloud cover and/or snow/ice.

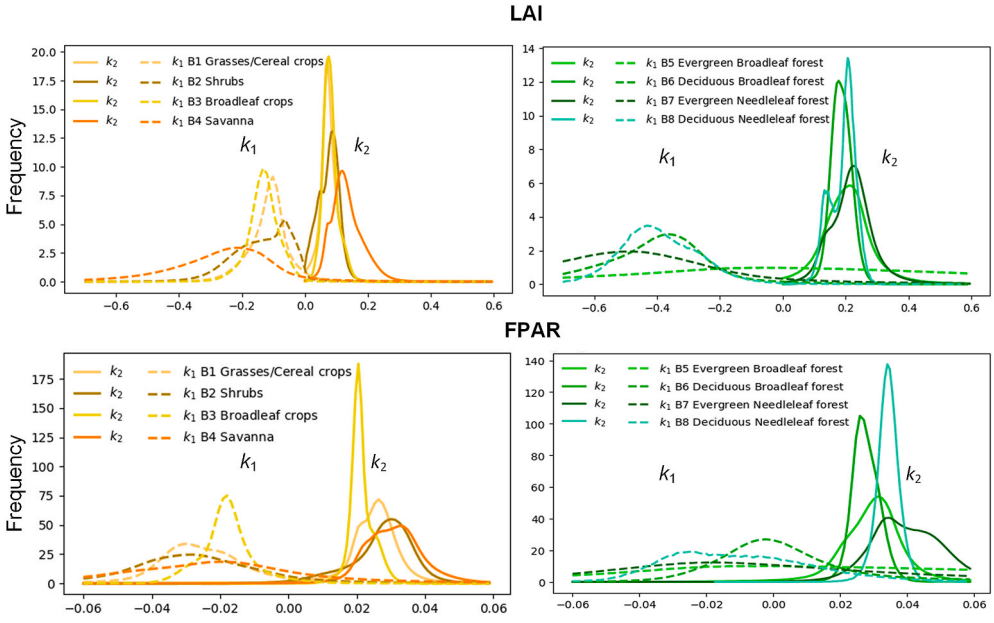

Fig. 13. Histograms of k_1 (dashed) and k_2 (solid) for MCD15A2H 8 biome classes, derived for LAI and FPAR.

very low R^2). To indicate the areas of non-applicability of the proposed parameterization we masked the areas with $R^2 < 0.5$ as well as where no data are available due to clouds or ice/snow in grey color. Fig. 14 (bottom) shows the global distribution of R^2 (for values above 0.5) indicating the areas of applicability of the proposed parameterization of vegetation variables. The areas with darker green correspond to higher R^2, that is the areas with the best performance of the proposed model for LAI (as well as FPAR). Naturally, these areas are agricultural lands and

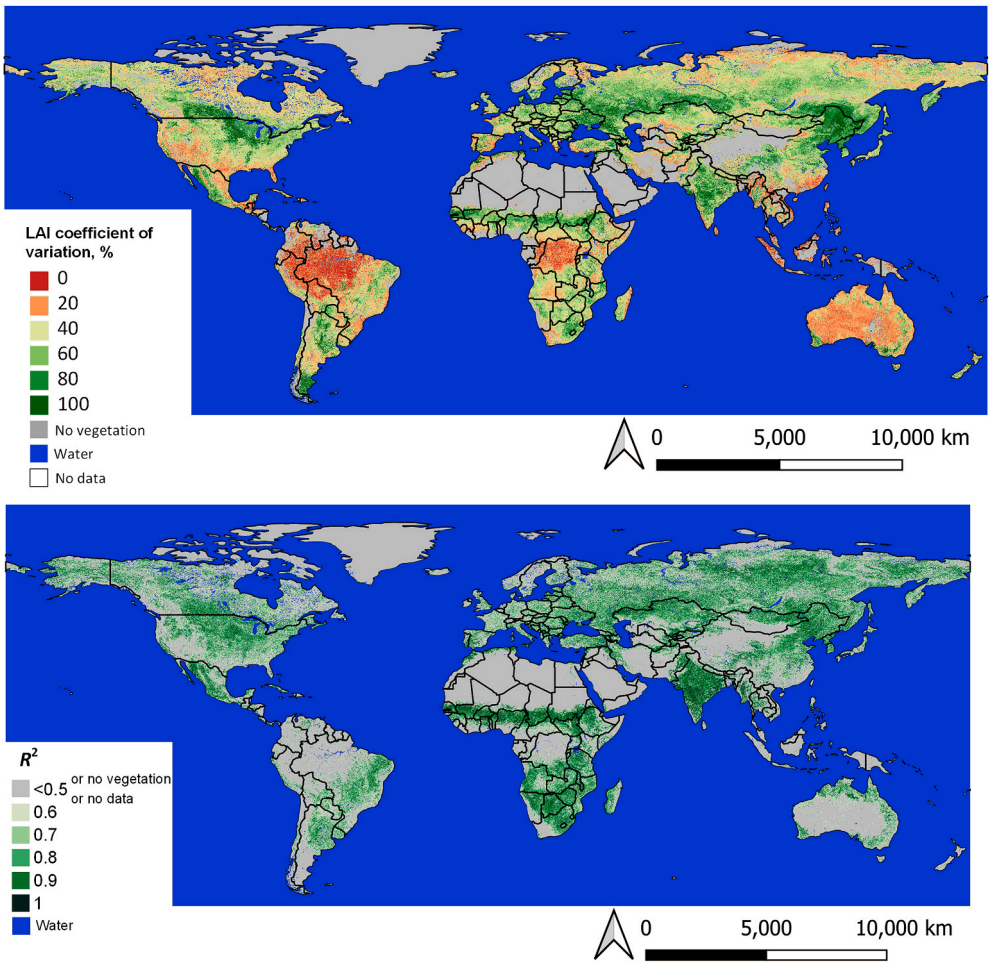

Fig. 14. Coefficient of variation of seasonal LAI for 2017 (top) and R^2 for the model $LAI = k_1\rho_1 + k_2\rho_2$ derived using MODIS data, where R^2>0.5 (bottom).

seasonal forests, corresponding to regions with substantial interannual variability (LAI Cov >40%).

5. Discussion and conclusions

This study proposes a rather simple, but effective, parameterization for vegetation variables LAI, FPAR and CCC. As a first step, we developed a two-parametric linear model based on the coefficients (or weights) for the red and NIR reflectances (Eq. (4)). Future investigations could further explore multi-parametric models, which may include other bands available on remote sensing sensors.

For convenience, we summarized k_1 and k_2 coefficients of agricultural crops derived using ground-based data, satellite and PROSAIL simulations for LAI (Fig. 15) and FPAR (Fig. 16). The coefficients for CCC were derived only for the Nebraska site (see Table 2). The LAI and FPAR ground observations were not available for forests, therefore the coefficients for forest classes were derived only from MODIS products (see Table 9), with the caveats mentioned earlier. Fig. 15 shows the k_1 and k_2 values obtained for the crops in Nebraska site, the CONUS territory (see Table 7), and for the global generic crops (cereal and broadleaf) used in MODIS products.

From Fig. 15 one can see that LAI regressions for crops based on ground and satellite observations (including those obtained using MODIS products) as well as PROSAIL model simulations yielded k_2 values all around 0.1, whereas k_1 values are between −0.1 and −0.3 (k_1 around −0.35 seems to be an outlier for wheat, derived from observations over Ukraine, yet to be understood).

The fact that both k_2 and k_1 values for FPAR model for all crops

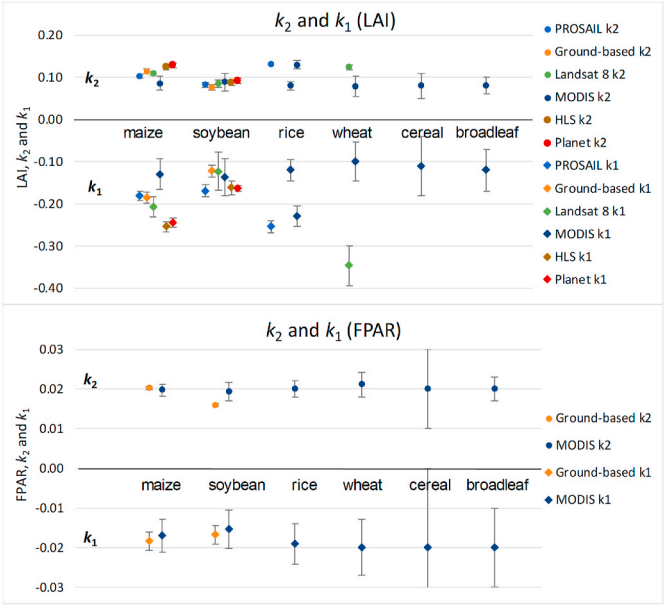

Fig. 15. A graphical summary of coefficients k_1 and k_2 for LAI and FPAR derived for crops using various datasets and simulation modelling.

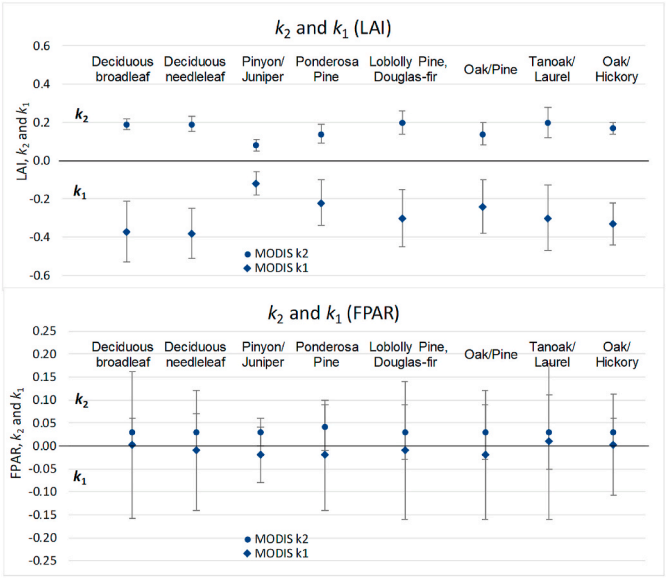

Fig. 16. A graphical summary of coefficients k_1 and k_2 for LAI and FPAR derived for forest using MODIS data.

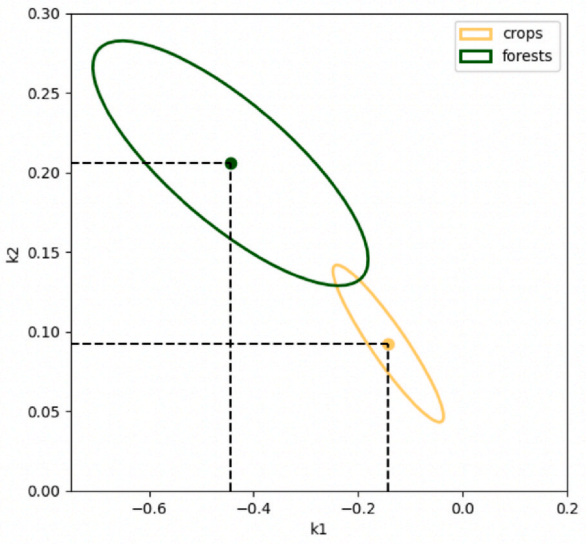

Fig. 17. The MODIS-derived forest and crop clusters of 2000 randomly selected data points for each cluster constrained by R^2>0.5 and LAI Cov>0.5 in k_1 x k_2 space. The data were fit to a 2D Gaussian distribution using covariance matrices, and then rotating the ellipse using eigen values.

considered (Fig. 15 bottom) are around 0.2 and −0.2, respectively, implies that a simple difference index DVI serves as a decent proxy for monitoring this biophysical variable over some crops, at least for those considered in this study. However, our results reveal that for forests (Fig. 16 bottom) DVI would be less appropriate in approximating FPAR, as the NIR reflectance should be weighted by at least 50% higher than the red reflectance.

Our analysis shows that although k_1 and k_2 for LAI estimation are relatively close, with k_2 around 0.1 and k_1 between −0.1 and −0.2 the difference could be substantial. The case in point is that for maize k_1 is around −0.2 whereas for soybean it is around −0.1, which suggests that the weights on the red and NIR reflectances may differ depending on the crop. This should be taken into account in studies that use combinations of red and NIR reflectances in simple indices, where the weights are prescribed equal.

We also learned that in the case of two observed crops in Nebraska (maize and soybean), the k_1 and k_2 values both LAI and CCC for maize are substantially higher than those for soybean whereas the ratio of coefficients or the slope *a*is quasi-invariant (around 1.6 ± 0.1, Table 7), suggesting relative independence of the crop type, at least for these two crops.

Using MODIS LAI product, we demonstrated that the patterns of k_2 coefficients correspond well to those of the known vegetation cover patterns over the globe while the values of the derived coefficients for the CONUS for crops are comparable to those derived from the ground-based measurements at the Nebraska and Ukraine sites. Some interesting tendencies in the derived coefficients for forests were explored and need to be further investigated using ground observations. As only MODIS LAI and FPAR products were used in deriving the coefficients for forest types, we stress the need of building and testing parameterizations with more ground observations in various forests. Summarizing our preliminary analysis of the histograms (Fig. 13) for areas with a reasonable model applicability, i.e. agricultural lands and seasonal forests (constrained by R^2>0.5 and LAI Cov>0.5), we tentatively conclude that there is a statistically significant separation of the coefficients for the two clusters, with MODIS data for forest types and crop types were clumped, respectively. Fig. 17 shows the two clusters as ellipses in k_1 x k_2 space, based on 2000 random samples per cluster for forest and crop biomes (see Fig. 12) with the means and two standard deviations of their distribution. It can be clearly seen that the weights on red and near-IR reflectances for estimating LAI in forests are roughly double of those corresponding values for crops.

Future improvements to the proposed two-parametric model could include generalization with more spectral bands, such as green and shortwave infrared, and others that are available on multi-spectral sensors. If thermal IR bands are to be used, a normalization of bands probably would be appropriate in building a parameterization. Note also that the soil factor is implicitly included in the parameterization but only for the available data which were used for building our model, i.e., the Nebraska sites. However, it is plausible that soil variability for the same crop in different areas may affect the regression coefficients. Comparison and validation for the Ukrainian site did not point at this factor but we leave this possibility for future research. Thus, more observations would refine the proposed parameters, which may become a function of soil. For this, additional information on soils would be required. The larger standard errors in k_1 may be attributable to nonlinearity observed in the functional dependence of red reflectance on both LAI and CCC (not shown here) for low values of these variables. Accounting for non-linearity may be another path for improvements of the proposed parameterization. A note of caution: the reader is reminded that the reflectances used in the parameterization are the normalized surface reflectances, i.e., if the data to be used for regressions are top-of-the-atmosphere reflectances, they need to be corrected for sun-target-sensor geometry and atmospheric effects.

Since the stability in time of the parameter coefficients was preliminarily verified for two crops, we hypothesize that this could be the case for all species. Thus, the proposed parameterization could be used for monitoring changes in biophysical variables using changes in reflectances with species-specific prescribed coefficients k_1 and k_2:

$$\partial V / \partial t = k_1 \partial \rho_1 / \partial t + k_2 \partial \rho_2 / \partial t,$$

where V is LAI, FPAR or CCC.

The proposed parameterization may prove attractive for global studies of various sub-classes of vegetation, once the parameter coefficients are established, validated, tabulated and their stability verified. Currently about 50 years of Landsat and 40 years of AVHRR time series data have been collected, hence once a global set of coefficients become available, this simple parameterization would provide quantification of vegetation traits for the past decades using AVHRR and Landsat time series. Climate models that use satellite-derived land cover classifications and land surface fluxes parameterizations, which include

vegetation variables, should benefit from the proposed parameterization.

In conclusion, we stress the importance that for further exploration of the proposed approach more ground observations of the above variables for various types of crops and forests would be required and hope that this study will motivate conducting such field experiments. Before the proposed parameterization is ready to be upscaled to a global level, much further research is required across a range of biomes using in situ measurements.

Declaration of competing interest

The authors declare that they have no known competing financial interests or personal relationships that could have appeared to influence the work reported in this paper.

Acknowledgements

Data provided by the Center for Advanced Land Management Information Technologies (CALMIT), the School of Natural Resources, and the Carbon Sequestration Program, all at the University of Nebraska-Lincoln, are greatly appreciated. We thank Timothy Arlkebauer, UNL, for sharing leaf area index data. Planet Lab is acknowledged for data over Nebraska. S. Skakun was supported by NASA [grant numbers 80NSSC18K0336, 80NSSC18M0039]. Thanks also go to Prof. Chris Justice (U. Maryland, USA) for reviewing the original manuscript, valuable comments and encouragement. We acknowledge productive interactions with Dr. Fred Baret (INRAE, France) and Dr. Jose Moreno (U. Valencia, Spain) at the early stage of this research. We appreciate constructive comments by anonymous reviewers that allowed us to substantially improve the manuscript. Finally, the lead author acknowledges the idea of using remotely sensed reflectances directly in land-surface parameterizations suggested by Prof. Roni Avissar (currently at U. Miami, Florida) about 25 years ago in personal communications.

References

Avissar, R., 1995. Recent advances in the representation of land-atmosphere interactions in general circulation models. Rev. Geophys. 33, 1005–1010.
Baret, F., Clevers, J.G.P.W., Steven, M.D., 1995. The robustness of canopy gap fraction estimates from red and near-infrared reflectances: a comparison of approaches. Rem. Sens. Environ. 54 (2), 141–151.
Baret, F., Guyot, G., 1991. Potentials and limits of vegetation indices for LAI and APAR assessment. Rem. Sens. Environ. 35 (2–3), 161–173.
Boryan, C., Yang, Z., Mueller, R., Craig, M., 2011. Monitoring US agriculture: the US department of agriculture, national agricultural statistics service, cropland data layer program. Geocarto Int. 26 (5), 341–358.
Broge, N.H., Leblanc, E., 2001. Comparing prediction power and stability of broadband and hyperspectral vegetation indices for estimation of green leaf area index and canopy chlorophyll density. Rem. Sens. Environ. 76 (2), 156–172.
Camps-Valls, Campos-Taberner, G.M., Moreno-Martínez, Á., Walther, S., Duveiller, G., Cescatti, A., Mahecha, M.D., Muñoz-Marí, J., García-Haro, F.J., Guanter, L., Jung, M., Gamon, J.A., Reichstein, M., Running, S.W., 2021. A unified vegetation index for quantifying the terrestrial biosphere. Science Advances 7 (9).
Ciganda, V., Gitelson, A., Schepers, J., 2009. Non-destructive determination of maize leaf and canopy chlorophyll content. J. Plant Physiol. 166 (2), 157–167.
Carrer, D., Roujean, J.-L., Lafont, S., Calvet, J.-C., Boone, A., Decharme, B., Delire, C., Gastellu-Etchegorry, J.P., 2013. A canopy radiative transfer scheme with explicit FAPAR for the interactive vegetation model ISBA-A-gs: impact on carbon fluxes. J. Geophys. Res.: Biogeosciences 118, 888–903.
Claverie, M., Ju, J., Masek, J.G., Dungan, J.L., Vermote, E.F., Roger, J.C., et al., 2018. The Harmonized Landsat and Sentinel-2 surface reflectance data set. Rem. Sens. Environ. 219, 145–161.
Clevers, J.G.P.W., 1989. The application of a weighted infra-red vegetation index for estimating leaf area index by correcting for soil moisture. Rem. Sens. Environ. 29, 25–37.
Clevers, J., Verhoeff, W., 1993. LAI estimation by means of the WDVI: a sensitivity analysis with a combined PROSPECT-SAIL model. Rem. Sens. Rev. 7, 43–64.
Crist, E.P., 1985. A TM tasseled cap equivalent transformation for reflectance factor data. Rem. Sens. Environ. 17 (3), 301–306.
Deardorff, J., 1978. Efficient prediction of ground temperature and moisture with inclusion of a layer of vegetation. J. Geophys. Res. 83, 1889–1903.
Fang, H., Liang, S., 2008. Leaf area index models. In: Jørgensen, S.E., Fath, B.D. (Eds.), Encyclopedia of Ecology, pp. 2139–2148.
Feret, J.-B., François, C., Asner, G.P., Gitelson, A.A., Martin, R.E., Bidel, L.P.R., Ustin, S. L., le Maire, G., Jacquemoud, S., 2008. PROSPECT-4 and 5: advances in the leaf optical properties model separating photosynthetic pigments. Rem. Sens. Environ. 112, 3030–3043.
Gitelson, A.A., 2013. Remote estimation of crop fractional vegetation cover: the use of noise equivalent as an indicator of performance of vegetation indices. Int. J. Rem. Sens. 34 (17), 6054–6066.
Gitelson, A., Arkebauer, T., Viña, A., Skakun, S., Inoue, Y., 2021. Evaluating plant photosynthetic traits via absorption coefficient in the photosynthetically active radiation region. Rem. Sens. Environ. 258, 112401.
Gitelson, A.A., Vina, A., Ciganda, V., Rundquist, D.C., Arkebauer, T., 2005. Remote estimation of canopy chlorophyll content in crops. Geophys. Res. Lett. 32 (8), L08403.
Gitelson, A., Viña, A., Solovchenko, A., Arkebauer, T., Inoue, Y., 2019. Derivation of canopy light absorption coefficient from reflectance spectra. Rem. Sens. Environ. 231, 111276.
Goward, S.N., Dye, D.G., Turner, S., Yang, J., 1993. Objective assessment of the NOAA global vegetation index data product. Int. J. Rem. Sens. 14, 3365–3394.
Gutman, G.G., 1990. Review of the workshop on the use of satellite-derived vegetation indices in weather and climate prediction model. Bull. Am. Meteorol. Soc. 71, 1458–1463.
Gutman, G.G., 1991. Vegetation indices from AVHRR: an update and future prospects. Rem. Sens. Environ. 35, 121–136.
Gutman, G.G., 1994. Global data on land surface parameters from NOAA AVHRR for use in numerical climate models. J. Clim. 7, 669–680.
Gutman, G., Ignatov, A., 1998. The derivation of the green vegetation fraction from NOAA/AVHRR data for use in numerical weather prediction models. Int. J. Rem. Sens. 19 (8), 1533–1543.
Holben, B.N., 1986. Characteristics of maximum-value composite images from temporal AVHRR data. Int. J. Rem. Sens. 7 (11), 1417–1434.
Huete, A.R., 1988. A soil-adjusted vegetation index (SAVI). Rem. Sens. Environ. 25, 53–70.
Ignatov, A., Gutman, G., 1999. Monthly mean diurnal cycles in surface temperature over land for global climate studies. J. Clim. 12, 1900–1910.
Inoue, Y., Guérif, M., Baret, F., Skidmore, A., Gitelson, A., Schlerf, M., Darvishzadeh, R., Olioso, A., 2016. Simple and robust methods for remote sensing of canopy chlorophyll content: a comparative analysis of hyperspectral data for different types of vegetation. Plant, Cell Environ 39 (12), 2609–2623.
Jacquemoud, S., Verhoef, W., Baret, F., Bacour, C., Zarco-Tejada, P.J., Asner, G.P., et al., 2009. PROSPECT+ SAIL models: a review of use for vegetation characterization. Rem. Sens. Environ. 113, S56–S66.
Johnson, D.M., Mueller, R., 2010. The 2009 cropland data layer. Photogramm. Eng. Rem. Sens. 76 (11), 1201–1205.
Jordan, C.F., 1969. Derivation of leaf-area index from quality of light on the forest floor. Ecology 50 (4), 663–666.
Kallel, A., Le Hégarat-Mascle, S., Ottle, C., Hubert-Moy, L., 2007. Determination of vegetation cover fraction by inversion of a four-parameter model based on isoline parametrization. Rem. Sens. Environ. 111 (4), 553–566.
Kang, Y., Özdoğan, M., Zipper, S.C., Román, M.O., Walker, J., Hong, S.Y., et al., 2016. How universal is the relationship between remotely sensed vegetation indices and crop leaf area index? A global assessment. Rem. Sens. 8 (7), 597.
Kauth, Thomas, 1976. The tasselled cap–a graphic description of the spectral-temporal development of agricultural crops as seen by Landsat. In: LARS Symposia, pp. 41–51 (paper 159).
Kriegler, F.J., Malila, W.A., Nalepka, R.F., Richardson, W., 1969. Preprocessing transformations and their effects on multispectral recognition. In: Proceedings of the Sixth International Symposium on Remote Sensing of Environment, pp. 97–131.
Knyazikhin, Y., Martonchik, J.V., Myneni, R.B., Diner, D.J., Running, S.W., 1998. Synergistic algorithm for estimating vegetation canopy leaf area index and fraction of absorbed photosynthetically active radiation from MODIS and MISR data. J. Geophys. Res.: Atmos. 103 (D24), 32257–32275.
Kussul, N., Skakun, S., Shelestov, A., Kussul, O., 2014. The use of satellite SAR imagery to crop classification in Ukraine within JECAM project. In: 2014 IEEE Geoscience and Remote Sensing Symposium. IEEE, New York, pp. 1497–1500.
Liu, L., Song, B., Zhang, S., Liu, X., 2017. A novel principal component analysis method for the reconstruction of leaf reflectance spectra and retrieval of leaf biochemical contents. Rem. Sens. 9 (11), 1113.
Los, S.O., Justice, C.O., Tucker, C.J., 1994. A global 1 by 1 NDVI data set for climate studies derived from the GIMMS continental NDVI data. Int. J. Rem. Sens. 15 (17), 3493–3518.
Myneni, R., Knyazikhin, Y., Park, T., 2015. MCD15A2H MODIS/Terra+Aqua leaf area index/FPAR 8-day L4 global 500m SIN grid V006. NASA EOSDIS Land Processes DAAC. https://doi.org/10.5067/MODIS/MCD15A2H.006.
Miranda, R., Nóbrega, R.L., Beserra de Moura, Raghavan, S., Galvíncio, J.D., 2020. Realistic and simplified models of plant and leaf area indices for a seasonally dry tropical forest. Int. J. Appl. Earth Observ. Geoinf. 85, 101992.
Morisette, J.T., Baret, F., Privette, J.L., Myneni, R.B., Nickeson, J.E., Garrigues, S., et al., 2006. Validation of global moderate-resolution LAI products: a framework proposed within the CEOS land product validation subgroup. IEEE Trans. Geosci. Rem. Sens. 44 (7), 1804–1817.
Nguy-Robertson, A.L., Gitelson, A.A., 2015. Algorithms for estimating green leaf area index in C3 and C4 crops for MODIS, Landsat TM/ETM+, MERIS, Sentinel MSI/OLCI, and Venμs sensors. Rem. Sens. Lett. 6 (5), 360–369.

Pearson, R.L., Miller, L.D., 1972. Remote mapping of standing crop biomass for estimation of the productivity of the shortgrass prairie. Rem. Sens. Environ. VIII,, 1355.
Pielke, R.A., Dalu, G.A., Snook, J.S., Lee, T.J., Kittel, T.G.F., 1991. Nonlinear influence of mesoscale land use on weather and climate. J. Clim. 4 (11), 1053–1069.
Planet Team, 2017. Planet application program interface: in space for life on earth. San Francisco, CA. https://api.planet.com.
Qi, J., Chehbouni, A., Huete, A.R., Kerr, Y.H., Sorooshian, A., 1994. A modified soil adjusted vegetation index. Rem. Sens. Environ. 48 (2), 119–126.
Reichstein, M., Camps-Valls, G., Stevens, B., Jung, M., Denzler, J., Carvalhais, N., 2019. Deep learning and process understanding for data-driven Earth system science. Nature 566 (7743), 195–204.
Richardson, A.J., Wiegand, C.L., 1977. Distinguishing vegetation from soil background information. Photogramm. Eng. Rem. Sens. 43 (12), 1541–1552.
Rouse, J.W., Haas, R.H., Schell, J.A., Deering, D.W., 1974. Monitoring vegetation systems in the Great Plains with ERTS. NASA special publication 351 (1974), 309.
Rundquist, D., Perk, R., Leavitt, B., Keydan, G., Gitelson, A., 2004. Collecting spectral data over cropland vegetation using machine-positioning versus hand-positioning of the sensor. Comput. Electron. Agric. 43 (2), 173–178.
Schaaf, C.B., Gao, F., Strahler, A.H., Lucht, W., Li, X., Tsang, T., et al., 2002. First operational BRDF, albedo nadir reflectance products from MODIS. Rem. Sens. Environ. 83 (1–2), 135–148.
Shelestov, A., Kolotii, A., Skakun, S., Baruth, B., Lozano, R.L., Yailymov, B., 2017. Biophysical parameters mapping within the SPOT-5 Take 5 initiative. Europ. J. Rem. Sens. 50 (1), 300–309.
Silleos, G.N., Alexandridis, T., Gitas, I.Z., Perakis, K., 2006. Vegetation indices: advances made in biomass estimation and vegetation monitoring in the last 30 years. Geocarto Int. 21 (4), 21–28.
Skakun, S., Kalecinski, N.I., Brown, M.G.L., Johnson, D.M., Vermote, E.F., Roger, J.-C., Franch, B., 2021. Assessing within-field corn and soybean yield variability from WorldView-3, Planet, sentinel-2, and Landsat 8 satellite imagery. Rem. Sens. 13, 872.
Skakun, S., Vermote, E., Franch, B., Roger, J.C., Kussul, N., Ju, J., Masek, J., 2019. Winter wheat yield assessment from Landsat 8 and sentinel-2 data: incorporating surface reflectance, through phenological fitting, into regression yield models. Rem. Sens. 11 (15), 1768.
Sellers, P.J., 1985. Canopy reflectance, photosynthesis and transpiration. Int. J. Rem. Sens. 6 (8), 1335–1372.
Sellers, P.J., Randall, D.A., Collatz, G.J., Berry, J.A., Field, C.B., Dazlich, D.A., Zhang, C., Bounoua, L., 1996. A revised land surface parameterization (SiB2) for atmospheric GCMs. Part I: model formulation. J. Clim. 9, 676–705.
Tucker, C.J., 1979. Red and photographic infrared linear combinations for monitoring vegetation. Rem. Sens. Environ. 8 (2), 127–150.
Tucker, C.J., Pinzon, J.E., Brown, M.E., Slayback, D.A., Pak, E.W., Mahoney, R., et al., 2005. An extended AVHRR 8-km NDVI dataset compatible with MODIS and SPOT vegetation NDVI data. Int. J. Rem. Sens. 26 (20), 4485–4498.
Verhoef, W., 1984. Light scattering by leaf layers with application to canopy reflectance modeling: the SAIL model. Rem. Sens. Environ. 16 (2), 125–141.
Verma, S.B., Dobermann, A., Cassman, K.G., Walters, D.T., Johannes, M., Knops, J.M., Arkebauer, T.J., et al., 2005. Annual carbon dioxide exchange in irrigated and rainfed maize-based agroecosystems. Agric. For. Meteorol. 131, 77–96.
Vermote, E., 2015. MOD09A1 MODIS surface reflectance 8-day L3 global 500m SIN grid V006. NASA EOSDIS Land Processes DAAC. https://doi.org/10.5067/MODIS/MOD09A1.006.
Vermote, E., Justice, C., Claverie, M., Franch, B., 2016. Preliminary analysis of the performance of the Landsat 8/OLI land surface reflectance product. Rem. Sens. Environ. 185, 46–56.
Vermote, E.F., Kotchenova, S., 2008. Atmospheric correction for the monitoring of land surfaces. J. Geophys. Res.: Atmos. 113 (D23).
Verrelst, J., Muñoz, J., Alonso, L., Delegido, J., Rivera, J.P., Camps-Valls, G., Moreno, J., 2012. Machine learning regression algorithms for biophysical parameter retrieval: opportunities for Sentinel-2 and-3. Rem. Sens. Environ. 118, 127–139.
Verrelst, J., Rivera, J.P., Gitelson, A., Delegido, J., Moreno, J., Camps-Valls, G., 2016. Spectral band selection for vegetation properties retrieval using Gaussian processes regression. Int. J. Appl. Earth Obs. Geoinf. 52, 554–567.
Viña, A., Gitelson, A.A., Nguy-Robertson, A.L., Peng, Y., 2011. Comparison of different vegetation indices for the remote assessment of green leaf area index of crops. Rem. Sens. Environ. 115 (12), 3468–3478.
Weiss, M., Baret, F., Smith, G.J., Jonckheere, I., Coppin, P., 2004. Review of methods for in situ leaf area index (LAI) determination: Part II. Estimation of LAI, errors and sampling. Agric. For. Meteorol. 121 (1–2), 37–53.
Yan, K., Park, T., Yan, G., Liu, Z., Yang, B., Chen, C., et al., 2016. Evaluation of MODIS LAI/FPAR product collection 6. Part 2: validation and intercomparison. Rem. Sens. 8 (6), 460.